Incremental Backstepping Sliding Mode Fault-Tolerant Flight Control

Wang, Xuerui; van Kampen, Erik-jan

DOI
10.2514/6.2019-0110

Publication date
2019

Document Version
Final published version

Published in
AIAA Scitech 2019 Forum

AIAA SciTech Forum
7-11 January 2019, San Diego, California
AIAA Scitech 2019 Forum

10.2514/6.2019-0110

Incremental Backstepping Sliding Mode Fault-Tolerant Flight Control

Xuerui Wang*, Erik-Jan van Kampen†
Delft University of Technology, Delft, Zuid-Holland, 2629HS, The Netherlands

Fault-tolerant flight control has the potential of improving the aircraft survivability in real life. This paper proposes an Incremental Backstepping Sliding Mode Control (IBSMC) framework for multi-input/output nonlinear strict-feedback systems considering model uncertainties, sudden faults, and external disturbances. This approach is a hybridization of the Sliding Mode Control (SMC) and a reformulated Incremental Backstepping (IBS). By virtue of the benefits contributed by both SMC and IBS, theoretical analyses prove IBSMC has less model dependency and enhanced robustness as compared to backstepping and backstepping hybridized with SMC (BSMC). When applied to an aircraft fault-tolerant control problem, numerical simulations demonstrate IBSMC can passively tolerate a wider range of model uncertainties, sudden actuator faults, and sudden structural damages as compared to backstepping and BSMC, using smooth control inputs with lower gains.

I. Introduction

Safety improvement is a timeless topic in the aerospace community. Over the past few decades, aircraft loss of control (LOC) has remained one of the key factors of fatal aircraft accidents [1, 2]. LOC is defined to include significant departure from the controlled operational flight envelop, which may be caused by inappropriate crew responses, aircraft impairments, icing, etc. [3]. To prevent loss of control, redundancies and fault tolerant features are strongly recommended in [3]. Fault-Tolerant Flight Control (FTFC), which is able to automatically maintain the stability and achieve acceptable level of performance in the presence of faults and disturbances with the remaining usable control effectors, is a promising approach to enhance aircraft survivability.

Backstepping is a nonlinear control method, which can globally stabilize strict-feedback systems though a recursive process [4, 5]. Due to its model-based nature, standard backstepping is sensitive to model mismatches. Adaptive Backstepping (ABS) integrated with parameter adaptive laws, such as Immersion and Invariance ABS [6], tuning functions ABS [7], can improve the system robustness to parametric uncertainties. However, the uncertainties need to be parameterized using pre-defined model structures, and the unknown parameters are normally required to be constant or slowly time-varying [8–10]. Moreover, when the system has high order, calculations of the virtual control in ABS can become complicate. Tuning the gains in the parameter update law can also be tedious. These issues constrain the applicability of ABS to FTFC problems, since the aerodynamic model structure is difficult to design, especially when structural damages occur. Furthermore, not all the uncertainties and disturbances can be parameterized and meet the slowly time-varying requirement at the same time. The high computational load of ABS is also unfavorable for FTFC systems.

Sliding Mode Control (SMC) [4, 5] is a type of variable structure control method featured by its robustness and easy implementation. External disturbances, parametric and nonparametric uncertainties are all incorporated into a lumped uncertainty term by SMC. Only the upper bound of this lumped uncertainty term is needed by conventional first-order SMC methods [11], while the upper bounds of the uncertainty derivatives are required by higher-order SMC methods [12, 13]. These requirements on knowledge of the bounds can further be removed by various Adaptive Sliding Mode Control (ASMC) methods [10, 14].

There have been continuous efforts in combining backstepping techniques with SMC to preserve the merits of both methods [8, 10, 14–17]. A second-order SMC is combined with ABS for feedback linearizable single-input/output (SISO) nonlinear systems that can be transformed into the parametric-pure feedback form and the parametric-strict feedback form in [8], where an SMC virtual control is included at the last step of the ABS design to improve robustness.

*PhD Candidate, Control and Simulation Section, Faculty of Aerospace Engineering, Delft University of Technology; Kluyverweg 1, 2629HS, Delft, The Netherlands. X.Wang-6@tudelft.nl, Student Member AIAA.

†Assistant Professor, Control and Simulation Section, Faculty of Aerospace Engineering, Delft University of Technology; Kluyverweg 1, 2629HS, Delft, The Netherlands, E.vanKampen@tudelft.nl, Member AIAA.

When the system can only be transformed to the semi-parametric strict feedback form, the SMC virtual control terms are needed in each recursive step to compensate for nonparametric uncertainties [15]. Dynamical ABS and SMC are hybridized in [16] for a class of SISO non-triangular nonlinear systems with unmatched parameterized uncertainties. In [17], integral backstepping is combined with conventional first-order SMC for a quadrotor trajectory control problem. In order to remove the pre-knowledge of the uncertainty bound, backstepping is hybridized with an ASMC method for a spacecraft attitude control problem in [10]. Adaptive fast terminal SMC with nonlinear sliding surface is incorporated into the backstepping framework for controlling the ducted fan engine of a thrust-vectored aircraft in [14]. In spite of the various SMC designs, the main idea of the combination is consistent in the above methods, that for the recursive steps encounter uncertainties, SMC virtual controls are incorporated into the baseline backstepping virtual control designs. Regarding the baseline backstepping methods, ABS is less suitable for FTFC as discussed before, while the (integral) backstepping has strong model dependency. A method that could reduce the model dependency of the baseline backstepping methods without adding extra computational load nor impairing robustness is desired.

Incremental Backstepping (IBS) is a sensor-based nonlinear control method, which can preserve the benefits of conventional backstepping control, while requiring less model knowledge. IBS was first proposed in [9], which was inspired by the Incremental Nonlinear Dynamic Inversion (INDI) method [18]. The only model information required by IBS is the control effectiveness matrix. To further improve the robustness of IBS to uncertainties in the control effectiveness matrix, on-line parameter update laws are incorporated into IBS in [9], while the tuning and compensation methods are introduced in [19]. Aircraft actuator jamming faults are passively tolerated by IBS in [20, 21]. Flight tests of a fixed-wing UAV under the control of command filtering IBS verified the robustness of this method to model uncertainties and disturbances [22]. Although IBS is a promising candidate for FTFC, its previous derivations based on the time-scale separation principle are not mathematically rigorous. The existing stability and robustness analyses for IBS also have limitations. These issues will be elaborated in subsection II.B.

The main contribution of this paper is the proposal of Incremental Backstepping Sliding Mode Control (IBSMC) framework for multi-input/output nonlinear strict-feedback systems under the perturbations of model uncertainties, on-board sudden faults, and external disturbances. First, the IBS method in the literature is reformulated for more general systems without using the time-scale separation principle. The IBSMC framework is then derived by incorporating the SMC virtual control into the IBS virtual control designs. As compared to SMC designs hybridized with backstepping (referred to as BSMC in this paper), theoretical analyses show IBSMC has not only less model dependency, but also enhanced robustness. This robustness enhancement is further verified numerically by an aircraft fault-tolerant control problem in the presence of model uncertainties, on-board sudden actuator faults and structural damages.

This paper is structured as follows: The derivations for backstepping, IBS, BSMC, IBSMC, and the analytical comparisons among them are presented in Sec. II. These methods are then applied to a fault-tolerant flight control problem in Sec. III. The robust performance of these methods are numerically compared in Sec. IV. Main conclusions are drawn in Sec. V.

II. Incremental Backstepping Sliding Mode Control

Consider a multi-input/output nonlinear uncertain system formulated by:

$$\begin{aligned}
\dot{\boldsymbol{x}}_1 &= \boldsymbol{f}_1(\boldsymbol{x}_1) + \boldsymbol{G}_1(\boldsymbol{x}_1)\boldsymbol{x}_2 \\
\dot{\boldsymbol{x}}_2 &= \boldsymbol{f}_2(\boldsymbol{x}_1, \boldsymbol{x}_2) + \boldsymbol{G}_2(\boldsymbol{x}_1, \boldsymbol{x}_2)\boldsymbol{x}_3 \\
&\vdots \\
\dot{\boldsymbol{x}}_n &= \boldsymbol{f}_n(\boldsymbol{x}_1, \boldsymbol{x}_2, ..., \boldsymbol{x}_n, \kappa(t)) + \boldsymbol{G}_n(\boldsymbol{x}_1, \boldsymbol{x}_2, ..., \boldsymbol{x}_n, \kappa(t))\boldsymbol{u} + \boldsymbol{d} \\
\boldsymbol{y} &= \boldsymbol{x}_1
\end{aligned} \tag{1}$$

where $\boldsymbol{x} = [\boldsymbol{x}_1^T, \boldsymbol{x}_2^T, ..., \boldsymbol{x}_n^T]^T$ is the state vector, with $\boldsymbol{x}_i \in \mathbb{R}^m,\ i = 1, 2, ..., n.\ \boldsymbol{u} \in \mathbb{R}^m$, $\boldsymbol{y} \in \mathbb{R}^m$ are the system input, output vectors. $\boldsymbol{f}_i \in \mathbb{R}^m,\ i = 1, 2, ...n-1$ is a set of smooth vector fields. $\boldsymbol{G}_i \in \mathbb{R}^{m\times m},\ i = 1, 2, ..., n-1$ is a set of smooth function mappings. The columns of each $\boldsymbol{G}_i$ are smooth vector fields. Assume $\boldsymbol{G}_i,\ i = 1, 2, ..., n-1$ are nonsingular. $\boldsymbol{f}_i,\ \boldsymbol{G}_i,\ i = 1, 2, ..., n-1$ are known dynamics. $\boldsymbol{d} \in \mathbb{R}^m$ represents external disturbance vector. $\boldsymbol{f}_n \in \mathbb{R}^m,\ \boldsymbol{G}_n \in \mathbb{R}^{m\times m}$ are perturbed by uncertainties and on-board faults, which are modeled as:

$$\boldsymbol{f}_n = \bar{\boldsymbol{f}}_n + (\boldsymbol{f}_f - \bar{\boldsymbol{f}}_n)\kappa(t) + \boldsymbol{\Phi}_n\boldsymbol{\theta} + \boldsymbol{\eta}_f(\boldsymbol{x}, t), \quad \boldsymbol{G}_n = \bar{\boldsymbol{G}}_n + (\boldsymbol{G}_f - \bar{\boldsymbol{G}}_n)\kappa(t) + \boldsymbol{\Psi}_n\boldsymbol{\theta} + \boldsymbol{\eta}_G(\boldsymbol{x}, t) \tag{2}$$

In the above equation, $\kappa(t) \in \mathbb{R}$ is designed as a step input to model the sudden fault at $t = t_f$ during flight. Specifically, $t < t_f,\ \kappa = 0$ indicates the fault-free case, and $t \geq t_f,\ \kappa = 1$ denotes post-fault condition. $\bar{\boldsymbol{f}}_n$ and $\bar{\boldsymbol{G}}_n$ are

the nominal models used for controller design, while $\boldsymbol{f}_f$ and $\boldsymbol{G}_f$ denoting the post-fault dynamics. $\bar{\boldsymbol{f}}_n,\ \boldsymbol{f}_f$ as well as the columns of $\bar{\boldsymbol{G}}_n, \boldsymbol{G}_f$ are smooth vector fields. $\boldsymbol{\Phi}_n\boldsymbol{\theta}$ and $\boldsymbol{\Psi}_n\boldsymbol{\theta}$ represent parametric uncertainties, where the parameter vector $\boldsymbol{\theta} \in \mathbb{R}^p$ is not necessarily constant nor slow time-varying. $\boldsymbol{\Phi}_n(\boldsymbol{x}), \boldsymbol{\Psi}_n(\boldsymbol{x}) \in \mathbb{R}^{m\times p}$, whose columns are known smooth vector fields. $\boldsymbol{\eta}_f,\ \boldsymbol{\eta}_G \in \mathbb{R}^m$ are smooth vector fields denoting nonparametric uncertainties. Assume $\boldsymbol{G}_n(\boldsymbol{x}, \kappa)$ is nonsingular. It will be shown in Sec. III that a class of aerospace system dynamics can be described by Eq. (1). More general cases where $\boldsymbol{f}_i,\ \boldsymbol{G}_i,\ i = 1, 2, ..., n-1$, also contain uncertainties will be elaborated in a follow-up paper.

A. Backstepping Sliding Mode Control

In this subsection, the Backstepping Sliding Mode Control (BSMC) will be derived for an output tracking problem. Denote the reference vector as $\boldsymbol{y}_r = [y_{r_1}, y_{r_2}, ..., y_{r_m}]^T$. Assume the derivatives of $y_{r_i}(t),\ i = 1, 2, ..., m$, up to $y_{r_i}^{(n)}(t)$ are continuous bounded functions, BSMC can be designed recursively as:

Step 1:

Define the error variable as $z_1 = \boldsymbol{x}_1 - \boldsymbol{y}_r$, recall Eq. (1), then:

$$\dot{z}_1 = \boldsymbol{f}_1 + \boldsymbol{G}_1\boldsymbol{x}_2 - \dot{\boldsymbol{y}}_r \tag{3}$$

This subsystem can be stabilized with respect to the candidate Lyapunov function $V_1(z_1) = \frac{1}{2}z_1^T z_1$ if $\boldsymbol{x}_2$ equals its desired value $\boldsymbol{x}_{2,d}$, which is designed as:

$$\boldsymbol{x}_{2,d} = \boldsymbol{\phi}_1(\boldsymbol{x}_1) = \boldsymbol{G}_1^{-1}(-\boldsymbol{f}_1 - \boldsymbol{K}_1 z_1 + \dot{\boldsymbol{y}}_r) \tag{4}$$

where $\boldsymbol{K}_1$ is a positive definite diagonal gain matrix. If $\boldsymbol{x}_2 = \boldsymbol{x}_{2,d}$, substituting Eq. (4) into Eq. (3) leads to:

$$\dot{V}_1(z_1) = -z_1^T\boldsymbol{K}_1 z_1 \leq \boldsymbol{0} \tag{5}$$

Step k ($2 \leq k \leq n-1$):

Define the tracking error of $\boldsymbol{x}_k$ as:

$$z_k = \boldsymbol{x}_k - \boldsymbol{x}_{k,d} \tag{6}$$

where $\boldsymbol{x}_{k,d} = \boldsymbol{\phi}_{k-1}(\boldsymbol{x}_1, ..., \boldsymbol{x}_{k-1})$ is the desired value for $\boldsymbol{x}_k$ designed in *Step k-1*. By using Eq. (1), the dynamics of z_k is given by:

$$\dot{z}_k = \boldsymbol{f}_k + \boldsymbol{G}_k\boldsymbol{x}_{k+1} - \dot{\boldsymbol{\phi}}_{k-1}(\boldsymbol{x}_1, ..., \boldsymbol{x}_{k-1}) \tag{7}$$

Design the desired value for $\boldsymbol{x}_{k+1}$ as:

$$\boldsymbol{x}_{k+1,d} = \boldsymbol{\phi}_k(\boldsymbol{x}_1, ..., \boldsymbol{x}_k) = \boldsymbol{G}_k^{-1}(-\boldsymbol{f}_k - \boldsymbol{K}_k z_k + \dot{\boldsymbol{\phi}}_{k-1} - \boldsymbol{G}_{k-1}^T z_{k-1}) \tag{8}$$

When $\boldsymbol{x}_{k+1} = \boldsymbol{x}_{k+1,d}$, by substituting Eq. (8) into Eq. (7), the time derivative of the candidate Lyapunov function $V_k(z_1, ..., z_k) = \frac{1}{2}\sum_{i=1}^{k} z_i^T z_i$ is derived as:

$$\dot{V}_k = -\sum_{i=1}^{k-1} z_i^T\boldsymbol{K}_i z_i + z_{k-1}^T\boldsymbol{G}_{k-1}z_k + z_k^T(-\boldsymbol{K}_k z_k - \boldsymbol{G}_{k-1}^T z_{k-1}) = -\sum_{i=1}^{k} z_i^T\boldsymbol{K}_i z_i \leq 0 \tag{9}$$

Step n:

Different from the above steps, model uncertainties, faults, and disturbances appear in the last step. Define the tracking error of $\boldsymbol{x}_n$ as:

$$z_n = \boldsymbol{x}_n - \boldsymbol{x}_{n,d} \tag{10}$$

Recall Eq. (1), the dynamics of z_n is given as:

$$\dot{z}_n = \boldsymbol{f}_n + \boldsymbol{G}_n\boldsymbol{u} + \boldsymbol{d} - \dot{\boldsymbol{\phi}}_{n-1} \tag{11}$$

Consider the candidate Lyapunov function as:

$$V_n = \frac{1}{2}\sum_{i=1}^{n} z_i^T z_i \tag{12}$$

The standard backstepping control input is design as:

$$\boldsymbol{u}_{bs} = \bar{\boldsymbol{G}}_n^{-1}(-\bar{\boldsymbol{f}}_n - \boldsymbol{K}_n\boldsymbol{z}_n + \dot{\boldsymbol{\phi}}_{n-1} - \boldsymbol{G}_{n-1}^T\boldsymbol{z}_{n-1}) \triangleq \bar{\boldsymbol{G}}_n^{-1}(\boldsymbol{\nu}_c - \bar{\boldsymbol{f}}_n) \tag{13}$$

in which the nominal models $\bar{\boldsymbol{f}}_n$ and $\bar{\boldsymbol{G}}_n$ are used. $\boldsymbol{\nu}_c$ denotes the continuous virtual control input. Substituting Eq. (13) into Eq. (12) yields:

$$\dot{V}_n = -\sum_{i=1}^{n} \boldsymbol{z}_i^T\boldsymbol{K}_i\boldsymbol{z}_i + \boldsymbol{z}_n^T(\boldsymbol{f}_n - \bar{\boldsymbol{f}}_n + (\boldsymbol{G}_n\bar{\boldsymbol{G}}_n^{-1} - \boldsymbol{I})(\boldsymbol{\nu}_c - \bar{\boldsymbol{f}}_n) + \boldsymbol{d}) \triangleq -\sum_{i=1}^{n} \boldsymbol{z}_i^T\boldsymbol{K}_i\boldsymbol{z}_i + \boldsymbol{z}_n^T\boldsymbol{\varepsilon}_{bs} \tag{14}$$

where $\boldsymbol{I} \in \mathbb{R}^{m\times m}$ is an identity matrix. $\boldsymbol{\varepsilon}_{bs}$ in the above equation indicates the uncertain vector that remains in the closed-loop system. If $\boldsymbol{\varepsilon}_{bs}$ is bounded, then $\boldsymbol{z}_i,\ i = 1, 2, ..., n$, can be proved to be ultimately bounded by class $\mathcal{K}$ functions of $\boldsymbol{\varepsilon}_{bs}$ [4, 23].

In order to improve the robustness of backstepping control, earlier research suggests combining Sliding Mode Control (SMC) with backstepping [8, 10, 14–17]. The main idea of this combination is to use a SMC virtual control input to compensate for the uncertain term $\boldsymbol{\varepsilon}_{bs}$. Normally, the BSMC is designed in the form of:

$$\boldsymbol{u}_{bsmc} = \bar{\boldsymbol{G}}_n^{-1}(\boldsymbol{\nu}_c + \boldsymbol{\nu}_s - \bar{\boldsymbol{f}}_n) \tag{15}$$

where $\boldsymbol{\nu}_s$ is the SMC virtual control input, which can be designed using any SMC technique. Design the sliding surface as $\boldsymbol{\sigma} = \boldsymbol{z}_n = \boldsymbol{0}$, then the classical design is $\boldsymbol{\nu}_s = -\boldsymbol{K}_s\text{sign}(\boldsymbol{\sigma}) = -[K_{s,1}\text{sign}(\sigma_1), K_{s,2}\text{sign}(\sigma_2), ..., K_{s,m}\text{sign}(\sigma_m)]^T,\ K_{s,i} > 0,\ i = 1, 2, ..., m$. Assume $\|\boldsymbol{I} - \boldsymbol{G}_n\bar{\boldsymbol{G}}_n^{-1}\| \le \bar{b} < 1$, and $\boldsymbol{\varepsilon}_{bs}$ is bounded, then by using Eq. (14), the time derivative of $V_n = \frac{1}{2}\sum_{i=1}^{n} \boldsymbol{z}_i^T\boldsymbol{z}_i$ using this BSMC is calculated by:

$$\begin{aligned}
\dot{V}_n &= -\sum_{i=1}^{n} \boldsymbol{z}_i^T\boldsymbol{K}_i\boldsymbol{z}_i + \boldsymbol{z}_n^T(\boldsymbol{\varepsilon}_{bs} - \boldsymbol{G}_n\bar{\boldsymbol{G}}_n^{-1}\boldsymbol{K}_s\text{sign}(\boldsymbol{\sigma})) \le -\sum_{i=1}^{n} \boldsymbol{z}_i^T\boldsymbol{K}_i\boldsymbol{z}_i + \sum_{i=1}^{m}(|\sigma_i||\varepsilon_{bs,i}| + \bar{b}K_{s,i}|\sigma_i| - K_{s,i}|\sigma_i|) \\
&\le -\sum_{i=1}^{n} \boldsymbol{z}_i^T\boldsymbol{K}_i\boldsymbol{z}_i - \sum_{i=1}^{m} \rho_i|\sigma_i|, \quad \forall K_{s,i} \ge \frac{\rho_i + |\varepsilon_{bs,i}|}{1-\bar{b}}, \quad \forall \rho_i > 0
\end{aligned} \tag{16}$$

According to Barbalat's Lemma [5], this BSMC design ensures $\boldsymbol{z}_i,\ i = 1, 2, ..., n$ and $\sigma_i,\ i = 1, 2, ..., m$ are asymptotically stable. Nonetheless, sign function is discontinuous, which leads to the chattering problem in practice. The boundary-layer method, which approximates the sign function by a saturation function, is a widely used approach to alleviate the chattering effect [4, 11]. Inside the boundary-layer, the control law becomes linear, so only asymptotic convergence is attained [4].

A Finite Reaching Time Continuous (FRTC) SMC method was proposed in [24, 25], which not only achieves finite time convergence to the sliding surface, but also has enhanced robustness to noise and disturbances as compared to the boundary-layer method [24]. This method will be elaborated in Sec. II.C.

B. Reformulation and Robustness Analysis for Incremental Backstepping

In order to improve the robustness of backstepping, the Incremental Backstepping (IBS) control was proposed in [26], and has been used for solving many flight control problems [9, 19–22, 26]. However, the existing derivations and robustness analyses of IBS have some limitations:

The core step of the existing IBS derivations is the model simplification based on the time-scale separation principle, which claims that the controls can change significantly faster than the states [9, 19–22, 26]. Based on this principle or assumption, when the sampling frequency is high, the state variation related nonlinear terms and higher-order terms are omitted from the Taylor series expansion of the nonlinear plant, which results in the simplified incremental dynamics used for controller design. This plant simplification is not mathematically rigorous since the states of an open-loop unstable plant may change faster that the controls. Furthermore, although the higher-order terms and state variation related terms are not used by the IBS control, they still exist in the closed-loop dynamics and remain influencing the closed-loop system stability and performance. These issues have been overlooked in the literature.

The existing robustness analyses of IBS also need improvements. It is straightforward concluded in [19], that systems under IBS control are robust to the uncertainties in system dynamics $\boldsymbol{f}_n(\boldsymbol{x})$, because the model of $\boldsymbol{f}_n(\boldsymbol{x})$ is not used in IBS designs. This statement is deficient since the influences of $\boldsymbol{f}_n(\boldsymbol{x})$ still remain in the closed-loop

system, although its model is not used by the controller. Moreover, Ref. [19] concludes if ideal actuators are used, the inner-loop system dynamics under IBS control is a single integrator, even when the control effectiveness matrix contains uncertainties. This conclusion is also defective because it is proved by using linear transfer functions derived from block diagrams, where the inappropriate condition $\dot{\boldsymbol{x}}_n = \dot{\boldsymbol{x}}_{n,0}$ is used. Last but not least, in [19], the stability and robustness of the closed-loop system under IBS control considering actuator dynamics are analyzed by formulating the closed-loop system into a state-space form, and testing the frozen-time eigenvalues of the time-varying system matrix. However, it has been proved in [27] that for the stability of Linear Time Varying (LTV) systems, the stability criterion based on the negative definiteness of the frozen-time eigenvalues is neither sufficient nor necessary.

Although the robustness of IBS to sudden actuator jamming faults has been numerically tested in [21], there is a lack of explicit theoretical analyses for the influences of sudden (discontinuous in time) faults on IBS. In addition, IBS in the literature is only derived for systems whose relative degree equal to two.

In view of these limitations of the existing IBS derivations, before the proposal of Incremental Backstepping Sliding Mode Control (IBSMC), the IBS control will be reformulated for more general systems (Eq. (1)) without using the time-scale separation principle. The stability of the closed-loop system will be analyzed using Lyapunov's method.

Taking the first-order Taylor series expansion for the dynamics of $\boldsymbol{x}_n$ around the previous sampled condition (denoted by the subscript 0) as:

$$\begin{aligned}\dot{\boldsymbol{x}}_n &= \dot{\boldsymbol{x}}_{n,0} + \left.\frac{\partial[\boldsymbol{f}_n(\boldsymbol{x},\kappa)+\boldsymbol{G}_n(\boldsymbol{x},\kappa)\boldsymbol{u}]}{\partial \boldsymbol{u}}\right|_0 \Delta\boldsymbol{u} + \left.\frac{\partial[\boldsymbol{f}_n(\boldsymbol{x},\kappa)+\boldsymbol{G}_n(\boldsymbol{x},\kappa)\boldsymbol{u}]}{\partial \boldsymbol{x}}\right|_0 \Delta\boldsymbol{x} + \left.\frac{\partial[\boldsymbol{f}_n(\boldsymbol{x},\kappa)+\boldsymbol{G}_n(\boldsymbol{x},\kappa)\boldsymbol{u}]}{\partial \kappa}\right|_0 \Delta\kappa \\ &\quad + \Delta\boldsymbol{d} + O(\Delta\boldsymbol{x}^2) \triangleq \dot{\boldsymbol{x}}_{n,0} + \boldsymbol{G}_n(\boldsymbol{x}_0,\kappa_0)\Delta\boldsymbol{u} + \Delta\boldsymbol{d} + \boldsymbol{\delta}(\boldsymbol{x},\kappa,\Delta t)\end{aligned} \tag{17}$$

where $\Delta\boldsymbol{x} = \boldsymbol{x} - \boldsymbol{x}_0$, $\Delta\boldsymbol{u} = \boldsymbol{u} - \boldsymbol{u}_0$, respectively denote the variations of states and control inputs in one incremental time step Δt. $\Delta\boldsymbol{d} = \boldsymbol{d} - \boldsymbol{d}_0$ denotes the variations of the external disturbances $\boldsymbol{d}$ in Δt, while $\Delta\kappa = \kappa - \kappa_0$ denotes the changes of the fault indicator κ. The remainder term $O(\Delta\boldsymbol{x}^2)$ is only a function of $\Delta\boldsymbol{x}^2$, since according to Eqs. (1, 2), $\frac{\partial^i \dot{\boldsymbol{x}}_n}{\partial \boldsymbol{u}^i} = \boldsymbol{0}$, $\frac{\partial^i \dot{\boldsymbol{x}}_n}{\partial \boldsymbol{d}^i} = \boldsymbol{0}$, $\frac{\partial^i \dot{\boldsymbol{x}}_n}{\partial \kappa^i} = \boldsymbol{0}$ for all $i \geq 2$. Referring to Eq. (17) as the incremental dynamic equation (without any simplification).

The derivations of IBS for *Step k,* $1 \leq k \leq n-1$ are the same as those of backstepping. The differences exist in *Step n*, in which the incremental dynamic equation will be used for the IBS controller design. The *Step n* for IBS is derived as:
Step n: Define the tracking error of $\boldsymbol{x}_n$ as:

$$\boldsymbol{z}_n = \boldsymbol{x}_n - \boldsymbol{x}_{n,d} \tag{18}$$

Using Eq. (17), the dynamics of $\boldsymbol{z}_n$ is given as:

$$\dot{\boldsymbol{z}}_n = \dot{\boldsymbol{x}}_{n,0} + \boldsymbol{G}_n(\boldsymbol{x}_0,\kappa_0)\Delta\boldsymbol{u} + \Delta\boldsymbol{d} + \boldsymbol{\delta}(\boldsymbol{x},\kappa,\Delta t) - \dot{\boldsymbol{\phi}}_{n-1} \tag{19}$$

Design the IBS control increment as:

$$\Delta\boldsymbol{u}_{ibs} = \bar{\boldsymbol{G}}_n^{-1}(-\dot{\boldsymbol{x}}_{n,0} - \boldsymbol{K}_n\boldsymbol{z}_n + \dot{\boldsymbol{\phi}}_{n-1} - \boldsymbol{G}_{n-1}^T\boldsymbol{z}_{n-1}) \triangleq \bar{\boldsymbol{G}}_n^{-1}(\boldsymbol{\nu}_c - \dot{\boldsymbol{x}}_{n,0}) \tag{20}$$

where the measurement/estimation of $\dot{\boldsymbol{x}}_{n,0}$ instead of the nominal model $\bar{\boldsymbol{f}}_n$ (Eq. (13)) is used by the controller. The total control command vector for actuators is $\boldsymbol{u}_{ibs} = \boldsymbol{u}_{ibs,0} + \Delta\boldsymbol{u}_{ibs}$.

Considering the same candidate Lyapunov function as Eq. (12), and substituting Eq. (20) into Eq. (12) yields:

$$\dot{V}_n = -\sum_{i=1}^{n} \boldsymbol{z}_i^T\boldsymbol{K}_i\boldsymbol{z}_i + \boldsymbol{z}_n^T(\boldsymbol{\delta}(\boldsymbol{x},\kappa,\Delta t) + (\boldsymbol{G}_n\bar{\boldsymbol{G}}_n^{-1} - \boldsymbol{I})(\boldsymbol{\nu}_c - \dot{\boldsymbol{x}}_{n,0}) + \Delta\boldsymbol{d}) \triangleq -\sum_{i=1}^{n} \boldsymbol{z}_i^T\boldsymbol{K}_i\boldsymbol{z}_i + \boldsymbol{z}_n^T\boldsymbol{\varepsilon}_{ibs} \tag{21}$$

In view of Eq. (21), the closed-loop system is perturbed by $\boldsymbol{\varepsilon}_{ibs}$, in which $\boldsymbol{\delta}(\boldsymbol{x},\kappa,\Delta t)$ contains the influences of sudden faults, state variation $\Delta\boldsymbol{x}$ related terms and higher-order terms. The term caused by control effectiveness matrix mismatches presents in $\boldsymbol{\varepsilon}_{ibs}$ even without considering actuator dynamics. The characteristics of $\boldsymbol{\varepsilon}_{ibs}$ will be further analyzed in subsection II.E.

C. Proposal of Incremental Backstepping Sliding Mode Control

As shown in Sec. II.B, the closed-loop system under IBS control is perturbed by $\boldsymbol{\varepsilon}_{ibs}$ when considering faults, uncertainties and disturbances. The influences of $\boldsymbol{\varepsilon}_{ibs}$ were also observed in the real-world flight tests of a fixed-wing UAV [22]. $\boldsymbol{\delta}(\boldsymbol{x},\kappa,\Delta t)$ and $\Delta\boldsymbol{d}$ are difficult to be parametrized, so it is less appropriate to use ABS for compensation. In

order to further improve the robustness of IBS, IBSMC will be proposed in this subsection. The control increment of IBSMC is designed in the form of:

$$\Delta \boldsymbol{u}_{ibsmc} = \bar{\boldsymbol{G}}_n^{-1}(\boldsymbol{\nu}_c + \boldsymbol{\nu}_s - \dot{\boldsymbol{x}}_{n,0}) \tag{22}$$

where $\boldsymbol{\nu}_c$ is the continuous IBS virtual control, which is identical to the $\boldsymbol{\nu}_c$ in Eq. (20). The SMC virtual control $\boldsymbol{\nu}_s$ can be designed using any SMC technique. In this subsection, the FRTC SMC method [24, 25] will be adopted. This method is essentially the same with the Terminal Sliding Mode (TSM) reaching law used in [28], which enforces finite time convergence to the sliding surface.

Design the sliding surface as $\boldsymbol{\sigma} = \boldsymbol{z}_n = \boldsymbol{0}$, and design $\boldsymbol{\nu}_s$ as:

$$\boldsymbol{\nu}_s = -\boldsymbol{K}_s \mathrm{sig}(\boldsymbol{\sigma})^{\boldsymbol{\gamma}} = -[K_{s,1}|\sigma_1|^{\gamma_1}\mathrm{sign}(\sigma_1), K_{s,2}|\sigma_2|^{\gamma_2}\mathrm{sign}(\sigma_2), ..., K_{s,m}|\sigma_m|^{\gamma_m}\mathrm{sign}(\sigma_m)]^T, \;\; i = 1, 2, ..., m \tag{23}$$

where $K_{s,i} > 0,\ \gamma_i \in (0, 1)$. It is noteworthy that $|\sigma_i|^{\gamma_i}\mathrm{sign}(\sigma_i)$ is a continuous function of σ_i without any approximation. Assume $\|\boldsymbol{I} - \boldsymbol{G}_n\bar{\boldsymbol{G}}_n^{-1}\| \le \bar{b} < 1$, and $\boldsymbol{\varepsilon}_{ibs}$ is bounded, then by using Eq. (21), the time derivative of $V_n = \frac{1}{2}\sum_{i=1}^{n} \boldsymbol{z}_i^T\boldsymbol{z}_i$ using IBSMC is calculated by:

$$\begin{aligned}
\dot{V}_n &= -\sum_{i=1}^{n} \boldsymbol{z}_i^T\boldsymbol{K}_i\boldsymbol{z}_i + \boldsymbol{z}_n^T(\boldsymbol{\varepsilon}_{ibs} - \boldsymbol{G}_n\bar{\boldsymbol{G}}_n^{-1}\boldsymbol{K}_s\mathrm{sig}(\boldsymbol{\sigma})^{\boldsymbol{\gamma}}) \le -\sum_{i=1}^{n} \boldsymbol{z}_i^T\boldsymbol{K}_i\boldsymbol{z}_i + \sum_{i=1}^{m}(|\sigma_i||\varepsilon_{ibs,i}| + \bar{b}K_{s,i}|\sigma_i|^{\gamma_i+1} - K_{s,i}|\sigma_i|^{\gamma_i+1}) \\
&\le -\sum_{i=1}^{n} \boldsymbol{z}_i^T\boldsymbol{K}_i\boldsymbol{z}_i - \sum_{i=1}^{m}\rho_i|\sigma_i|, \qquad \forall|\sigma_i| \ge \left(\frac{\rho_i + |\varepsilon_{ibs,i}|}{(1-\bar{b})K_{s,i}}\right)^{\frac{1}{\gamma_i}}, \quad \forall\rho_i > 0
\end{aligned} \tag{24}$$

Eq. (24) proves the Domain of Attraction (DOA) [4] of σ_i equals $\left(\frac{\rho_i+|\varepsilon_{ibs,i}|}{(1-\bar{b})K_{s,i}}\right)^{\frac{1}{\gamma_i}}$, whose size can be made arbitrarily small when $K_{s,i} > \frac{\rho_i+|\varepsilon_{ibs,i}|}{(1-\bar{b})}$, and if γ_i is arbitrarily small. Define $\boldsymbol{z} = [\boldsymbol{z}_1^T, \boldsymbol{z}_1^T, ..., \boldsymbol{z}_n^T]^T$, since $V_n = \frac{1}{2}\|\boldsymbol{z}\|_2^2$, and $\boldsymbol{\sigma} = \boldsymbol{z}_n$, Eq. (24) also proves $\boldsymbol{z}$ is uniformly ultimately bounded [4, 23].

D. Other Sliding Surface Designs

The sliding variable $\boldsymbol{\sigma}$ is not necessarily equal to $\boldsymbol{z}_n$, it can also be a linear or nonlinear function of $\boldsymbol{z}_i$, for example:

$$\boldsymbol{\sigma} = \boldsymbol{z}_n + \boldsymbol{C}_{n-1}\boldsymbol{z}_{n-1} + \boldsymbol{C}_{n-2}\boldsymbol{z}_{n-2} + ... + \boldsymbol{C}_1\boldsymbol{z}_1 \tag{25}$$

Design the candidate Lyapunov function as:

$$V = \frac{1}{2}\sum_{i=1}^{n-1} \boldsymbol{z}_i^T\boldsymbol{z}_i + \frac{1}{2}\boldsymbol{\sigma}^T\boldsymbol{\sigma} \tag{26}$$

Both BSMC and IBSMC methods can be used to stabilize V. Reviewing Sec. II.A and II.C, it can be seen that the control input derivations for *Step k,* $1 \le k \le n-1$ are the same as in the standard backstepping design, and the closed-loop system dynamics are given as:

$$\begin{aligned}
\dot{\boldsymbol{z}}_1 &= \boldsymbol{f}_1 + \boldsymbol{G}_1\boldsymbol{x}_{2,d} - \dot{\boldsymbol{y}}_r + \boldsymbol{G}_1\boldsymbol{z}_2 = -\boldsymbol{K}_1\boldsymbol{z}_1 + \boldsymbol{G}_1\boldsymbol{z}_2 \\
\dot{\boldsymbol{z}}_i &= \boldsymbol{f}_i + \boldsymbol{G}_i\boldsymbol{x}_{i+1,d} - \dot{\boldsymbol{\phi}}_{i-1} + \boldsymbol{G}_i\boldsymbol{z}_{i+1} = -\boldsymbol{K}_i\boldsymbol{z}_i - \boldsymbol{G}_{i-1}^T\boldsymbol{z}_{i-1} + \boldsymbol{G}_i\boldsymbol{z}_{i+1}, \;\; 2 \le i \le n-1
\end{aligned} \tag{27}$$

Using Eqs. (25, 27), the dynamics of the sliding variable are derived as:

$$\dot{\boldsymbol{\sigma}} = \boldsymbol{C}_1(-\boldsymbol{K}_1\boldsymbol{z}_1 + \boldsymbol{G}_1\boldsymbol{z}_2) + \sum_{i=2}^{n-1}\boldsymbol{C}_i(-\boldsymbol{K}_i\boldsymbol{z}_i - \boldsymbol{G}_{i-1}^T\boldsymbol{z}_{i-1} + \boldsymbol{G}_i\boldsymbol{z}_{i+1}) + \dot{\boldsymbol{z}}_n \tag{28}$$

The derivative of the candidate Lyapunov function (Eq. (26)) is derived using Eqs. (25, 27, 28, 1) as:

$$\begin{aligned}
\dot{V} &= -\sum_{i=1}^{n-1} \boldsymbol{z}_i^T\boldsymbol{K}_i\boldsymbol{z}_i + \boldsymbol{z}_{n-1}^T\boldsymbol{G}_{n-1}\boldsymbol{z}_n + \boldsymbol{\sigma}^T\dot{\boldsymbol{\sigma}} \\
&= -\sum_{i=1}^{n-1} \boldsymbol{z}_i^T\boldsymbol{K}_i\boldsymbol{z}_i - \boldsymbol{z}_{n-1}^T\boldsymbol{G}_{n-1}(\boldsymbol{C}_{n-1}\boldsymbol{z}_{n-1} + ... + \boldsymbol{C}_1\boldsymbol{z}_1) + \boldsymbol{z}_{n-1}^T\boldsymbol{G}_{n-1}\boldsymbol{\sigma} \\
&\quad + \boldsymbol{\sigma}^T[\boldsymbol{C}_1(-\boldsymbol{K}_1\boldsymbol{z}_1 + \boldsymbol{G}_1\boldsymbol{z}_2) + \sum_{i=2}^{n-1}\boldsymbol{C}_i(-\boldsymbol{K}_i\boldsymbol{z}_i - \boldsymbol{G}_{i-1}^T\boldsymbol{z}_{i-1} + \boldsymbol{G}_i\boldsymbol{z}_{i+1}) + (\boldsymbol{f}_n + \boldsymbol{G}_n\boldsymbol{u} + \boldsymbol{d} - \dot{\boldsymbol{\phi}}_{n-1})]
\end{aligned} \tag{29}$$

An SMC virtual control term $\boldsymbol{\nu}_s$ is needed to compensator for the uncertainties, faults and disturbances present in $\dot{\boldsymbol{z}}_n$. Design the control input of BSMC as:

$$\begin{aligned}\boldsymbol{u}_{bsmc} &= \bar{\boldsymbol{G}}_n^{-1}(-\bar{\boldsymbol{f}}_n + \dot{\boldsymbol{\phi}}_{n-1} - \boldsymbol{G}_{n-1}^T \boldsymbol{z}_{n-1} - \boldsymbol{C}_1(-\boldsymbol{K}_1\boldsymbol{z}_1 + \boldsymbol{G}_1\boldsymbol{z}_2) - \sum_{i=2}^{n-1}\boldsymbol{C}_i(-\boldsymbol{K}_i\boldsymbol{z}_i - \boldsymbol{G}_{i-1}^T\boldsymbol{z}_{i-1} + \boldsymbol{G}_i\boldsymbol{z}_{i+1}) - \boldsymbol{K}_c\boldsymbol{\sigma} + \boldsymbol{\nu}_s) \\ &\triangleq \bar{\boldsymbol{G}}_n^{-1}(\boldsymbol{\nu}_c' + \boldsymbol{\nu}_s - \bar{\boldsymbol{f}}_n) \end{aligned} \tag{30}$$

where $\boldsymbol{K}_c$ is a positive definite gain matrix.

Analogous to the previous control designs, $\boldsymbol{\nu}_s$ can be designed using any SMC technique. As an example, following the classical way as $\boldsymbol{\nu}_s = -\boldsymbol{K}_s\text{sign}(\boldsymbol{\sigma})$, where $\boldsymbol{K}_s$ is a positive definite diagonal gain matrix. Denote $\boldsymbol{\varepsilon}_{bs}' = \boldsymbol{f}_n - \bar{\boldsymbol{f}}_n + (\boldsymbol{G}_n\bar{\boldsymbol{G}}_n^{-1} - \boldsymbol{I})(\boldsymbol{\nu}_c' - \boldsymbol{f}_n) + \boldsymbol{d}$. Assume $\|\boldsymbol{I} - \boldsymbol{G}_n\bar{\boldsymbol{G}}_n^{-1}\| \le \bar{b} < 1$, and $\boldsymbol{\varepsilon}_{bs}'$ is bounded, then substituting Eq. (30) into Eq. (29) results in:

$$\begin{aligned}\dot{V} &= -\sum_{i=1}^{n-1}\boldsymbol{z}_i^T\boldsymbol{K}_i\boldsymbol{z}_i - \boldsymbol{z}_{n-1}^T\boldsymbol{G}_{n-1}(\boldsymbol{C}_{n-1}\boldsymbol{z}_{n-1} + ... + \boldsymbol{C}_1\boldsymbol{z}_1) + \boldsymbol{\sigma}^T(\boldsymbol{\varepsilon}_{bs}' - \boldsymbol{K}_c\boldsymbol{\sigma} - \boldsymbol{G}_n\bar{\boldsymbol{G}}_n^{-1}\boldsymbol{K}_s\text{sign}(\boldsymbol{\sigma})) \\ &\le -[\boldsymbol{z}_1^T, \boldsymbol{z}_2^T, ..., \boldsymbol{z}_{n-1}^T]\begin{bmatrix}\boldsymbol{K}_1 & \boldsymbol{0} & ... & \boldsymbol{0} \\ \boldsymbol{0} & \boldsymbol{K}_2 & ... & \boldsymbol{0} \\ \vdots & \vdots & \vdots & \vdots \\ \boldsymbol{G}_{n-1}\boldsymbol{C}_1 & \boldsymbol{G}_{n-1}\boldsymbol{C}_2 & ... & \boldsymbol{G}_{n-1}\boldsymbol{C}_{n-1} + \boldsymbol{K}_{n-1}\end{bmatrix}\begin{bmatrix}\boldsymbol{z}_1 \\ \boldsymbol{z}_2 \\ \vdots \\ \boldsymbol{z}_{n-1}\end{bmatrix} \\ &\quad -\boldsymbol{\sigma}^T\boldsymbol{K}_c\boldsymbol{\sigma} + \sum_{i=1}^{m}(|\sigma_i||\varepsilon_{bs,i}'| + \bar{b}K_{s,i}|\sigma_i| - K_{s,i}|\sigma_i|) \\ &\le -[\boldsymbol{z}_1^T, \boldsymbol{z}_2^T, ..., \boldsymbol{z}_{n-1}^T]\boldsymbol{Q}[\boldsymbol{z}_1^T, \boldsymbol{z}_2^T, ..., \boldsymbol{z}_{n-1}^T]^T - \boldsymbol{\sigma}^T\boldsymbol{K}_c\boldsymbol{\sigma} - \sum_{i=1}^{m}\rho_i|\sigma_i|, \quad \forall K_{s,i} \ge \frac{\rho_i + |\varepsilon_{bs,i}'|}{1-\bar{b}}, \ \forall\rho_i > 0 \end{aligned} \tag{31}$$

$\dot{V} \le 0$ if $\boldsymbol{Q}$ is a positive definite matrix, which can be achieved by properly choosing $\boldsymbol{C}_i$ and $\boldsymbol{K}_i$. If the positive definiteness of $\boldsymbol{Q}$ is achieved, then according to Barbalat's Lemma [5], $z_i,\ i = 1, 2, ..., n-1$, and $\boldsymbol{\sigma}$ asymptotically converge to zero.

By contrast, design the IBSMC input as:

$$\begin{aligned}\Delta\boldsymbol{u}_{ibsmc} &= \bar{\boldsymbol{G}}_n^{-1}(-\dot{\boldsymbol{x}}_{n,0} + \dot{\boldsymbol{\phi}}_{n-1} - \boldsymbol{G}_{n-1}^T\boldsymbol{z}_{n-1} - \boldsymbol{C}_1(-\boldsymbol{K}_1\boldsymbol{z}_1 + \boldsymbol{G}_1\boldsymbol{z}_2) - \sum_{i=2}^{n-1}\boldsymbol{C}_i(-\boldsymbol{K}_i\boldsymbol{z}_i - \boldsymbol{G}_{i-1}^T\boldsymbol{z}_{i-1} + \boldsymbol{G}_i\boldsymbol{z}_{i+1}) - \boldsymbol{K}_c\boldsymbol{\sigma} + \boldsymbol{\nu}_s) \\ &\triangleq \bar{\boldsymbol{G}}_n^{-1}(\boldsymbol{\nu}_c' + \boldsymbol{\nu}_s - \dot{\boldsymbol{x}}_{n,0}) \end{aligned} \tag{32}$$

Design $\boldsymbol{\nu}_s = -\boldsymbol{K}_s\text{sign}(\boldsymbol{\sigma})$, in which $\boldsymbol{K}_s$ is a positive definite diagonal matrix. Assume $\|\boldsymbol{I} - \boldsymbol{G}_n\bar{\boldsymbol{G}}_n^{-1}\| \le \bar{b} < 1$, and $\boldsymbol{\varepsilon}_{ibs}' = \boldsymbol{\delta}(\boldsymbol{x}, \kappa, \Delta t) + (\boldsymbol{G}_n\bar{\boldsymbol{G}}_n^{-1} - \boldsymbol{I})(\boldsymbol{\nu}_c' - \dot{\boldsymbol{x}}_{n,0}) + \Delta\boldsymbol{d}$ is bounded, then the time derivative of Eq. (26) under the control of Eq. (32) is derived as:

$$\dot{V} \le -[\boldsymbol{z}_1^T, \boldsymbol{z}_2^T, ..., \boldsymbol{z}_{n-1}^T]\boldsymbol{Q}[\boldsymbol{z}_1^T, \boldsymbol{z}_2^T, ..., \boldsymbol{z}_{n-1}^T]^T - \boldsymbol{\sigma}^T\boldsymbol{K}_c\boldsymbol{\sigma} - \sum_{i=1}^{m}\rho_i|\sigma_i|, \quad \forall K_{s,i} \ge \frac{\rho_i + |\varepsilon_{ibs,i}'|}{1-\bar{b}}, \ \forall\rho_i > 0 \tag{33}$$

Using Barbalat's Lemma [5], $z_i,\ i = 1, 2, ..., n-1$, and $\boldsymbol{\sigma}$ are asymptotically stable if $\boldsymbol{Q}$ is positive definite, which can be achieved by properly designing $\boldsymbol{C}_i$ and $\boldsymbol{K}_i$.

E. Comparisons between BSMC and IBSMC

In this subsection, the BSMC designed in Sec. II.A and the IBSMC designed in Sec. II.C will be compared analytically. The main focus of the comparisons are on the control structure, thus the conclusions draw in this subsection are not constrained by the specific SMC virtual control design. In other words, the sliding variable can be any function of z_i, and $\boldsymbol{\nu}_s$ in Eqs. (15, 22) can be designed using any SMC technique, as long as the same SMC method is consistently used by BSMC and IBSMC for fair comparisons.

The first difference between BSMC and IBSMC can be revealed by Eqs. (15, 22), where the nominal model $\bar{\boldsymbol{f}}_n$ is used by BSMC, while the measurements or estimations of $\dot{\boldsymbol{x}}_{n,0}$ and $\boldsymbol{u}_0$ are needed by IBSMC. Consequently, IBSMC has less model dependency than BSMC, but is more sensitive to sensing issues (e.g., sensor noise, delays, etc.).

In Eqs. (15, 22), the SMC virtual control $\boldsymbol{\nu}_s$ is used to compensate for $\boldsymbol{\varepsilon}_{bs}$ and $\boldsymbol{\varepsilon}_{ibs}$. Using Eqs. (13, 14, 2), $\boldsymbol{\varepsilon}_{bs}$ can be written as:

$$\begin{aligned}\boldsymbol{\varepsilon}_{bs} &= \boldsymbol{f}_n - \bar{\boldsymbol{f}}_n + (\boldsymbol{G}_n\bar{\boldsymbol{G}}_n^{-1} - \boldsymbol{I})(\boldsymbol{\nu}_c - \boldsymbol{f}_n) + \boldsymbol{d} \\ &= \boldsymbol{f}_n - \bar{\boldsymbol{f}}_n + (\boldsymbol{G}_n - \bar{\boldsymbol{G}}_n)\boldsymbol{u}_{bs} + \boldsymbol{d} \\ &= [\boldsymbol{\Phi}_n\boldsymbol{\theta} + \boldsymbol{\eta}_f + (\boldsymbol{\Psi}_n\boldsymbol{\theta} + \boldsymbol{\eta}_G)\boldsymbol{u}_{bs} + \boldsymbol{d}] + [(\boldsymbol{f}_f - \bar{\boldsymbol{f}}_n) + (\boldsymbol{G}_f - \bar{\boldsymbol{G}}_n)\boldsymbol{u}_{bs}]\kappa(t)\end{aligned} \tag{34}$$

For the IBSMC method, using Eq. (2), the $\boldsymbol{\delta}(\boldsymbol{x}, \kappa, \Delta t)$ in Eq. (17) can be further derived as:

$$\boldsymbol{\delta}(\boldsymbol{x}, \kappa, \Delta t) = \boldsymbol{\delta}_b(\boldsymbol{x}, \Delta t) + \boldsymbol{\delta}_d(\boldsymbol{x}, \Delta t)\kappa_0 + \boldsymbol{\delta}_\kappa(\boldsymbol{x})\Delta\kappa \tag{35}$$

where

$$\begin{aligned}\boldsymbol{\delta}_b(\boldsymbol{x}, \Delta t) &= \left.\frac{\partial[\bar{\boldsymbol{f}}_n + \boldsymbol{\Phi}_n\boldsymbol{\theta} + \boldsymbol{\eta}_f + (\bar{\boldsymbol{G}}_n + \boldsymbol{\Psi}_n\boldsymbol{\theta} + \boldsymbol{\eta}_G)\boldsymbol{u}_{ibs}]}{\partial\boldsymbol{x}}\right|_0 \Delta\boldsymbol{x} + O(\Delta\boldsymbol{x}^2) \\ \boldsymbol{\delta}_d(\boldsymbol{x}, \Delta t) &= \left.\frac{\partial[(\boldsymbol{f}_f - \bar{\boldsymbol{f}}_n) + (\boldsymbol{G}_f - \bar{\boldsymbol{G}}_n)\boldsymbol{u}_{ibs}]}{\partial\boldsymbol{x}}\right|_0 \Delta\boldsymbol{x} \\ \boldsymbol{\delta}_\kappa(\boldsymbol{x}) &= [(\boldsymbol{f}_f - \bar{\boldsymbol{f}}_n) + (\boldsymbol{G}_f - \bar{\boldsymbol{G}}_n)\boldsymbol{u}_{ibs}]|_0\end{aligned} \tag{36}$$

Therefore, using Eqs. (20, 35) the uncertain vector $\boldsymbol{\varepsilon}_{ibs}$ in Eq. (21) can be rewritten as:

$$\begin{aligned}\boldsymbol{\varepsilon}_{ibs} &= \boldsymbol{\delta}(\boldsymbol{x}, \kappa, \Delta t) + (\boldsymbol{G}_n\bar{\boldsymbol{G}}_n^{-1} - \boldsymbol{I})(\boldsymbol{\nu}_c - \dot{\boldsymbol{x}}_{n,0}) + \Delta\boldsymbol{d} \\ &= \boldsymbol{\delta}(\boldsymbol{x}, \kappa, \Delta t) + (\boldsymbol{G}_n - \bar{\boldsymbol{G}}_n)\Delta\boldsymbol{u}_{ibs} + \Delta\boldsymbol{d} \\ &= [\boldsymbol{\delta}_b + (\boldsymbol{\Psi}_n\boldsymbol{\theta} + \boldsymbol{\eta}_G)\Delta\boldsymbol{u}_{ibs} + \Delta\boldsymbol{d}] + [\boldsymbol{\delta}_d\kappa_0 + (\boldsymbol{G}_f - \bar{\boldsymbol{G}})\Delta\boldsymbol{u}_{ibs}\kappa(t)] + \boldsymbol{\delta}_\kappa\Delta\kappa\end{aligned} \tag{37}$$

Since $\boldsymbol{x}_i,\ i = 1, 2, ..., n$ are continuous functions of t, $\lim_{\Delta t\to 0}\|\Delta\boldsymbol{x}\| = 0$. Assume that all order partial derivatives of $\boldsymbol{f}_n(\boldsymbol{x}, \kappa)$ and $\boldsymbol{G}_n(\boldsymbol{x}, \kappa)$ with respect to $\boldsymbol{x}$ are bounded, recall Eq. (36), the perturbation terms satisfy:

$$\lim_{\Delta t\to 0}\|\boldsymbol{\delta}_b(\boldsymbol{x}, \Delta t)\| = 0, \quad \lim_{\Delta t\to 0}\|\boldsymbol{\delta}_d(\boldsymbol{x}, \Delta t)\| = 0, \quad \forall\boldsymbol{x}_i \in \mathbb{R}^m,\ i = 1, 2, ..., n \tag{38}$$

Eq. (38) indicates that the norm of these perturbation terms become negligible for sufficiently high sampling frequency [23]. Eq. (38) also indicates that $\forall\bar{\delta}_\varepsilon > 0, \exists\Delta\bar{t} > 0, s.t.\ \forall\Delta t \in (0, \Delta\bar{t}],\ \forall\boldsymbol{x}_i \in \mathbb{R}^m,\ i = 1, 2, ..., n,\ \|\boldsymbol{\delta}_b(\boldsymbol{x}, \Delta t)\| \leq \bar{\delta}_\varepsilon,\ \|\boldsymbol{\delta}_d(\boldsymbol{x}, \Delta t)\| \leq \bar{\delta}_\varepsilon$. In other words, there exists a Δt that ensures the boundedness of both $\boldsymbol{\delta}_b(\boldsymbol{x}, \Delta t)$ and $\boldsymbol{\delta}_d(\boldsymbol{x}, \Delta t)$. Also, their bounds can be further reduced by increasing the sampling frequency. Inspired by the analysis for the boundedness of the residual error under incremental nonlinear dynamic inversion control in [29], the following theorem is proposed for the boundedness of $\boldsymbol{\varepsilon}_{ibs}$:

Theorem 1 *If $\|\boldsymbol{I} - \boldsymbol{G}_n\bar{\boldsymbol{G}}_n^{-1}\| \leq \bar{b} < 1$ for all t, and if $\boldsymbol{\delta}_\kappa(\boldsymbol{x})$ is bounded when $t_f \leq t < t_f + \Delta t$, for sufficiently high sampling frequency, $\boldsymbol{\varepsilon}_{ibs}$ given by Eq. (37) is ultimately bounded.*

Proof: Using Eqs. (17, 20, 37), the closed-loop system dynamics under IBS control are:

$$\dot{\boldsymbol{x}}_n = \dot{\boldsymbol{x}}_{n,0} + \boldsymbol{G}_n\bar{\boldsymbol{G}}_n^{-1}(\boldsymbol{\nu}_c - \dot{\boldsymbol{x}}_{n,0}) + \Delta\boldsymbol{d} + \boldsymbol{\delta}(\boldsymbol{x}, \kappa, \Delta t) = \boldsymbol{\nu}_c + \boldsymbol{\varepsilon}_{ibs} \tag{39}$$

This equation is valid at every time step, thus for the previous time step, $\dot{\boldsymbol{x}}_{n,0} = \boldsymbol{\nu}_{c_0} + \boldsymbol{\varepsilon}_{ibs_0}$. Recall Eq. (37), $\boldsymbol{\varepsilon}_{ibs}$ can then be derived as:

$$\begin{aligned}\boldsymbol{\varepsilon}_{ibs} &= (\boldsymbol{G}_n\bar{\boldsymbol{G}}_n^{-1} - \boldsymbol{I})(\boldsymbol{\nu}_c - \boldsymbol{\nu}_{c_0} - \boldsymbol{\varepsilon}_{ibs_0}) + \boldsymbol{\delta}(\boldsymbol{x}, \kappa, \Delta t) + \Delta\boldsymbol{d} \\ &= (\boldsymbol{I} - \boldsymbol{G}_n\bar{\boldsymbol{G}}_n^{-1})\boldsymbol{\varepsilon}_{ibs_0} - (\boldsymbol{I} - \boldsymbol{G}_n\bar{\boldsymbol{G}}_n^{-1})(\boldsymbol{\nu}_c - \boldsymbol{\nu}_{c_0}) + \boldsymbol{\delta} + \Delta\boldsymbol{d} \\ &\triangleq \boldsymbol{E}\boldsymbol{\varepsilon}_{ibs_0} - \boldsymbol{E}\Delta\boldsymbol{\nu}_c + \boldsymbol{\delta} + \Delta\boldsymbol{d}\end{aligned} \tag{40}$$

which can be written in a recursive way as:

$$\boldsymbol{\varepsilon}_{ibs}(k) = \boldsymbol{E}(k)\boldsymbol{\varepsilon}_{ibs}(k-1) - \boldsymbol{E}(k)\Delta\boldsymbol{\nu}_c(k) + \boldsymbol{\delta}(k) + \Delta\boldsymbol{d}(k) \tag{41}$$

In view of Eq. (20), $\boldsymbol{\nu}_c$ is a continuous function of time, thus

$$\lim_{\Delta t\to 0} \|\boldsymbol{\nu}_c - \boldsymbol{\nu}_{c_0}\| = 0, \quad \forall \boldsymbol{x}_i \in \mathbb{R}^m \tag{42}$$

Therefore, for a sufficiently high sampling frequency, $\Delta\boldsymbol{\nu}_c$ is bounded. Since $\kappa(t)$ is a step function to indicate a sudden fault at $t = t_f$, $\Delta\kappa$ is a single square pulse with magnitude of one and width of Δt. As a result, $\boldsymbol{\delta}_\kappa(\boldsymbol{x})\Delta\kappa$ in Eq. (35) is bounded if $\boldsymbol{\delta}_\kappa(\boldsymbol{x})$ is bounded when $t_f \le t < t_f + \Delta t$. Furthermore, using Eqs. (35, 38), if $\boldsymbol{\delta}_\kappa(\boldsymbol{x})\Delta\kappa$ is bounded, then there exists a Δt which ensures the boundedness of $\boldsymbol{\delta}(\boldsymbol{x}, \kappa, \Delta t)$. In addition, disturbance increment $\Delta\boldsymbol{d}$ in real-world is normally bounded. Denote the bounds for $\Delta\boldsymbol{\nu}_c$, $\boldsymbol{\delta}$, and $\Delta\boldsymbol{d}$ as $\overline{\Delta\nu}_c$, $\bar{\delta}$, and $\overline{\Delta d}$ respectively, then Eq. (41) satisfies:

$$\begin{aligned}
\|\boldsymbol{\varepsilon}_{ibs}(k)\| &\le (\bar{b})^k\|\boldsymbol{\varepsilon}_{ibs}(0)\| + \sum_{j=1}^{k}(\bar{b})^{k-j+1}\|\Delta\boldsymbol{\nu}_c(j)\| + \sum_{j=1}^{k-1}(\bar{b})^{k-j}\|\boldsymbol{\delta}(j) + \Delta\boldsymbol{d}(j)\| + \|\boldsymbol{\delta}(j) + \Delta\boldsymbol{d}(j)\| \\
&\le (\bar{b})^k\|\boldsymbol{\varepsilon}_{ibs}(0)\| + \overline{\Delta\nu}_c\sum_{j=1}^{k}(\bar{b})^{k-j+1} + (\bar{\delta} + \overline{\Delta d})\sum_{j=1}^{k-1}(\bar{b})^{k-j} + (\bar{\delta} + \overline{\Delta d}) \\
&= (\bar{b})^k\|\boldsymbol{\varepsilon}_{ibs}(0)\| + \overline{\Delta\nu}_c\frac{\bar{b} - \bar{b}^{k+1}}{1-\bar{b}} + (\bar{\delta} + \overline{\Delta d})\frac{1-\bar{b}^k}{1-\bar{b}}
\end{aligned} \tag{43}$$

Since $\bar{b} < 1$, Eq. (43) satisfies:

$$\|\boldsymbol{\varepsilon}_{ibs}\| \le \frac{\overline{\Delta\nu}_c\bar{b} + \bar{\delta} + \overline{\Delta d}}{1-\bar{b}}, \quad \text{as } k \to \infty \tag{44}$$

In conclusion, $\boldsymbol{\varepsilon}_{ibs}$ is bounded for all k, and is ultimately bounded by $\frac{\overline{\Delta\nu}_c\bar{b}+\bar{\delta}+\overline{\Delta d}}{1-\bar{b}}$. □

For the majority of SMC designs, the boundedness of uncertainties is a precondition. Theorem 1 proves that a diagonally dominate structure of $\boldsymbol{G}_n\bar{\boldsymbol{G}}_n^{-1}$, bounded $\boldsymbol{\delta}_\kappa(\boldsymbol{x})$ when $t_f \le t < t_f + \Delta t$, and a sufficiently high sampling frequency ensure the boundedness of $\boldsymbol{\varepsilon}_{ibs}$. However, as a function of both $\boldsymbol{x}$ and $\boldsymbol{u}_{bs}$, and being independent of Δt, the boundedness of $\boldsymbol{\varepsilon}_{bs}$ is undetermined in the same conditions. Even for some moderate fault and disturbance circumstances, where both $\boldsymbol{\varepsilon}_{bs}$ and $\boldsymbol{\varepsilon}_{ibs}$ are bounded, it will be shown subsequently that $\boldsymbol{\varepsilon}_{ibs}$ has smaller bound, which can be further diminished by increasing the sampling frequency.

Denote the fault instant as $t = t_f$, the values of $\boldsymbol{\varepsilon}_{bs}$ and $\boldsymbol{\varepsilon}_{ibs}$ will be analyzed in three cases:

1) Pre-fault $t < t_f$: $\kappa(t) = 0$, $\kappa(t - \Delta t) = \kappa_0 = 0$, $\Delta\kappa = 0$.
2) Fault instant $t_f \le t < t_f + \Delta t$: $\kappa(t) = 1$, $\kappa(t - \Delta t) = \kappa_0 = 0$, $\Delta\kappa = 1$.
3) Post-fault $t \ge t_f + \Delta t$: $\kappa(t) = 1$, $\kappa(t - \Delta t) = \kappa_0 = 1$, $\Delta\kappa = 0$.

Recall Eqs. (34, 37), when $t < t_f$, $\boldsymbol{\varepsilon}_{bs} = \boldsymbol{\Phi}_n\boldsymbol{\theta} + \boldsymbol{\eta}_f + (\boldsymbol{\Psi}_n\boldsymbol{\theta} + \boldsymbol{\eta}_G)\boldsymbol{u}_{bs} + \boldsymbol{d}$, while $\boldsymbol{\varepsilon}_{ibs} = \boldsymbol{\delta}_b + (\boldsymbol{\Psi}_n\boldsymbol{\theta} + \boldsymbol{\eta}_G)\Delta\boldsymbol{u}_{ibs} + \Delta\boldsymbol{d}$. $\boldsymbol{\Phi}_n\boldsymbol{\theta}$ and $\boldsymbol{\eta}_f$ are the parametric and nonparametric uncertain terms of $\boldsymbol{f}_n$. For aerospace systems, $\|\boldsymbol{\Phi}_n\boldsymbol{\theta} + \boldsymbol{\eta}_f\|$ is normally large because it contains the inertia and aerodynamic uncertainties. By contrast, as a function of Δt, $\|\boldsymbol{\delta}_b\|$ can become negligible as formulated by Eq. (38). If $\|\boldsymbol{u}_{bs}\| \neq \boldsymbol{0}$ and $\|\boldsymbol{\Psi}_n\boldsymbol{\theta} + \boldsymbol{\eta}_G\| \neq \boldsymbol{0}$, there exists a Δt that ensures $\|\boldsymbol{\Psi}_n\boldsymbol{\theta} + \boldsymbol{\eta}_G\|\|\Delta\boldsymbol{u}_{ibs}\| < \|\boldsymbol{\Psi}_n\boldsymbol{\theta} + \boldsymbol{\eta}_G\|\|\boldsymbol{u}_{bs}\|$. In addition, most external disturbances in real-world are continuous functions of time, thus $\lim_{\Delta t\to 0}\|\Delta\boldsymbol{d}\| = 0$. Equivalently, when $\boldsymbol{d} \neq \boldsymbol{0}$, $\exists\Delta t, s.t.\ \|\Delta\boldsymbol{d}\| < \|\boldsymbol{d}\|$. The influences of discontinuous $\boldsymbol{d}$ (such as a bird strike or a sudden collision) can be analyzed in the same way as that of $\kappa(t)$. In summary, when $t < t_f$, in the presence of perturbations, if $\|\boldsymbol{u}_{bs}\| \neq \boldsymbol{0}$, then there exists a Δt that ensures $\boldsymbol{\varepsilon}_{ibs}$ has smaller bound.

During the short time interval $t_f \le t < t_f + \Delta t$, according to Eqs. (34, 37), an additional term $(\boldsymbol{f}_f - \bar{\boldsymbol{f}}_n) + (\boldsymbol{G}_f - \bar{\boldsymbol{G}}_n)\boldsymbol{u}_{bs}$ is added to $\boldsymbol{\varepsilon}_{bs}$, while $(\boldsymbol{G}_f - \bar{\boldsymbol{G}}_n)\Delta\boldsymbol{u}_{ibs} + \boldsymbol{\delta}_\kappa$ is added to $\boldsymbol{\varepsilon}_{ibs}$. These two additional terms have comparable bounds.

For the post-fault condition, $\boldsymbol{\varepsilon}_{bs}$ is still augmented by $(\boldsymbol{f}_f - \bar{\boldsymbol{f}}_n) + (\boldsymbol{G}_f - \bar{\boldsymbol{G}}_n)\boldsymbol{u}_{bs}$, while $\boldsymbol{\delta}_d + (\boldsymbol{G}_f - \bar{\boldsymbol{G}})\Delta\boldsymbol{u}_{ibs}$ is added to $\boldsymbol{\varepsilon}_{ibs}$. This reveals a feature of IBSMC, that the term $\boldsymbol{\delta}_\kappa(\boldsymbol{x})\Delta\kappa$ is only non-zero during a short time interval $t_f \le t < t_f + \Delta t$. After $t = t_f + \Delta t$, the main influences of fault have already been included by the measurements/estimations at the previous time step. Although $(\boldsymbol{G}_f - \bar{\boldsymbol{G}}_n)\Delta\boldsymbol{u}_{ibs}$ still remains after the fault, analogous to the analyses for the pre-fault condition, if $\|\boldsymbol{u}_{bs}\| \neq \boldsymbol{0}$, there exists a Δt that ensures $\|\boldsymbol{G}_f - \bar{\boldsymbol{G}}_n\|\|\Delta\boldsymbol{u}_{ibs}\| < \|\boldsymbol{G}_f - \bar{\boldsymbol{G}}_n\|\|\boldsymbol{u}_{bs}\|$. Furthermore, $\|\boldsymbol{f}_f - \bar{\boldsymbol{f}}_n\|$ evaluates the dynamic variations caused by faults, which is non-ignorable in faulty conditions. By contrast, $\|\boldsymbol{\delta}_d\|$ can become

negligible for a sufficient small Δt (Eq. (38)). Therefore, after a fault occurs, if $\|\boldsymbol{u}_{bs}\| \neq \boldsymbol{0}$, then there exists a Δt that ensures $\boldsymbol{\varepsilon}_{ibs}$ has smaller bound.

In summary, the conditions in Theorem 1 ensure a bounded $\boldsymbol{\varepsilon}_{ibs}$, while the boundedness of $\boldsymbol{\varepsilon}_{bs}$ is undetermined in the same conditions. For the fault and disturbance circumstances where both $\boldsymbol{\varepsilon}_{bs}$ and $\boldsymbol{\varepsilon}_{ibs}$ are bounded, if the sampling frequency is sufficient high, $\|\boldsymbol{\varepsilon}_{ibs}\|$ is smaller than $\|\boldsymbol{\varepsilon}_{bs}\|$ before and after a fault occurs, and can be further reduced by increasing the sampling frequency. This smaller $\|\boldsymbol{\varepsilon}_{ibs}\|$ can fundamentally release the control effort of SMC, since for most SMC designs, the required SMC gains are monotonically increasing functions of the uncertainty bounds. As a consequence, inheriting the robustness of both IBS and SMC, IBSMC is able to attain better robust performance using not only less model information, but also reduced SMC gains as compared to BSMC. These conclusions will be numerically validated in Sec. IV. A reasonable choice of the sampling frequency depends on the specific system characteristics and hardware constraints [23]. It has been proved by flight tests that 50∼100 Hz is suitable for airplane flight control [22, 30].

III. Fault-Tolerant Flight Control System Design

In this section, the control methods derived for generic nonlinear uncertain systems (Eq. (1) in Sec. II) will be applied to fault-tolerant flight control problems.

A. Aircraft Dynamics

The six degrees of freedom nonlinear equations of motion for rigid aircraft expressed in the body-fixed frame are given by:

$$\begin{bmatrix} \dot{\boldsymbol{V}} \\ \dot{\boldsymbol{\omega}} \end{bmatrix} = \begin{bmatrix} m\boldsymbol{I} & \boldsymbol{0} \\ \boldsymbol{0} & \boldsymbol{J} \end{bmatrix}^{-1} \begin{bmatrix} -m\tilde{\boldsymbol{\omega}}\boldsymbol{V} + \boldsymbol{F} \\ -\tilde{\boldsymbol{\omega}}\boldsymbol{J}\boldsymbol{\omega} + \boldsymbol{M} \end{bmatrix} \tag{45}$$

where $\boldsymbol{V} = [u, v, w]^T$ and $\boldsymbol{\omega} = [p, q, r]^T$ represent the translation and rotational velocities of the body-fixed frame relative to the inertial frame. m is the total mass. $\boldsymbol{J}$ represents the inertia matrix. $\tilde{(\cdot)}$ denotes the skew symmetric matrix of the corresponding vector. $\boldsymbol{F}$ and $\boldsymbol{M}$ are the total force and moment vectors, which incorporate gravitational, aerodynamic, and thrust forces and moments.

A typical aerodynamic model for a fixed-wing aircraft is give in the form of:

$$\begin{aligned} \boldsymbol{M}_a &= q_\infty S \mathrm{diag}([b, \bar{c}, b]) \left(\begin{bmatrix} C_l(\beta, r, p, M) \\ C_m(\alpha, q, M) \\ C_n(\beta, r, p, M) \end{bmatrix} + \begin{bmatrix} C_{l_{\delta_a}}(\alpha, \beta, M) & 0 & C_{l_{\delta_r}}(\alpha, \beta, M) \\ 0 & C_{m_{\delta_e}}(\alpha, M) & 0 \\ C_{n_{\delta_a}}(\alpha, \beta, M) & 0 & C_{n_{\delta_r}}(\alpha, \beta, M) \end{bmatrix} \begin{bmatrix} \delta_a \\ \delta_e \\ \delta_r \end{bmatrix} \right) \\ \boldsymbol{F}_a &= q_\infty S [C_x(\alpha, \beta, q, \delta_e, M), \quad C_y(\alpha, \beta, p, r, \delta_a, \delta_r, M), \quad C_z(\alpha, \beta, q, \delta_e, M)]^T \end{aligned} \tag{46}$$

where α, β represent the angle of attack and the sideslip angle. M is the Mach number. V is the airspeed. The dynamic pressure is given by $q_\infty = 0.5\rho_a V^2$ (ρ_a is the air density). $S, b, \bar{c}$ are the wing area, wing span and mean aerodynamic chord respectively.

Referring to the definition $\beta = \arcsin \frac{v}{V}$, the dynamics of β is derived as:

$$\dot{\beta} = \frac{V\dot{v} - v\dot{V}}{V\sqrt{u^2 + w^2}} \tag{47}$$

Denote the specific force vector as $\boldsymbol{A} = [A_x, A_y, A_z]^T$, and express the gravitational vector in the body-fixed frame as $\boldsymbol{G} = [-g \sin\theta, g \sin\phi \cos\theta, g \cos\phi \cos\theta]^T$, where g is the gravitational acceleration. Using Eq. (45, 47), the kinematic equations for β is derived as:

$$\dot{\beta} = \left(\frac{1}{\sqrt{u^2 + w^2}} \right) (F_{\beta,x} + F_{\beta,y} + F_{\beta,z}) + \begin{bmatrix} \frac{w}{\sqrt{u^2 + w^2}} & 0 & \frac{-u}{\sqrt{u^2 + w^2}} \end{bmatrix} [p \; q \; r]^T \tag{48}$$

where

$$\begin{aligned} F_{\beta,x} &= -\frac{uv}{V^2}(A_x - g\sin\theta) \\ F_{\beta,y} &= (1-\frac{v^2}{V^2})(A_y + g\sin\phi\cos\theta) \\ F_{\beta,z} &= -\frac{vw}{V^2}(A_z + g\cos\theta\cos\theta) \end{aligned} \tag{49}$$

The kinematics for Euler angles $[\phi, \theta, \psi]^T$ are given by:

$$\begin{bmatrix} \dot{\phi} \\ \dot{\theta} \\ \dot{\psi} \end{bmatrix} = \begin{bmatrix} 1 & \sin\phi\tan\theta & \cos\phi\tan\theta \\ 0 & \cos\phi & -\sin\phi \\ 0 & \frac{\sin\phi}{\cos\theta} & \frac{\cos\phi}{\cos\theta} \end{bmatrix} \begin{bmatrix} p \\ q \\ r \end{bmatrix} \tag{50}$$

B. Model for Aircraft Actuator Faults

Three types of actuator faults will be modeled in this subsection: partial loss of control effectiveness, solid jamming, and solid Oscillatory Failure Case (OFC).

The partial loss of control effectiveness can be modeled by multiplying the control derivatives with an scaling factor, namely, $C'_{i_j} = \mu_j C_{i_j},\ i = l, m, n,\ j = \delta_a, \delta_e, \delta_r,\ \mu_j \in (0, 1]$, with $(\cdot)'$ indicating the post-fault condition.

Solid jamming means the control surface is stuck at a certain position. The word "solid" is used to distinguish this fault case from liquid jamming, which means an additive bias presents in the rod sensor while the control surface is still movable. There are three main effects of control surface solid jamming. The first one is the loss of control effectiveness, namely if one side of the aileron or elevator is stuck, the corresponding control derivatives are halved, i.e. $\mu_j = 0.5, j = \delta_a, \delta_e$. Solid jamming fault also introduces new control derivatives, which invalidate the decoupling between longitudinal and lateral control. To be specific, one-side aileron jamming introduces $C_{m_{\delta_a}}$, while one-side elevator jamming introduces $C_{l_{\delta_e}}$ and $C_{n_{\delta_e}}$. Besides, if control surfaces are jammed at non-neutral positions, extra force and moment coefficients $(\tilde{C}_x, \tilde{C}_y, \tilde{C}_z, \tilde{C}_l, \tilde{C}_m, \tilde{C}_n)$ will be induced. These coefficients are functions of the aircraft geometry parameters, and are also proportional to the jammed positions [29].

The solid OFC is mainly caused by electronic components in fault mode generating spurious sinusoidal signals, which propagate through the servo-loop control, and lead to control surface oscillations [31]. "solid" means the spurious sinusoidal signals substitute instead of being added to ("liquid" OFC) the normal control signal [31]. Similar to the effects of control surface solid jamming, if one-side of elevator or aileron has solid OFC, the corresponding control derivatives are halved. New coupled control derivatives are also introduced. Moreover, the disturbing force and moment coefficients $(\tilde{C}_x, \tilde{C}_y, \tilde{C}_z, \tilde{C}_l, \tilde{C}_m, \tilde{C}_n)$ induced by solid OFC are also spurious sinusoidal signals.

C. Model for Aircraft Structural Damages

Aircraft structural damages result in three main effects: actuator faults, the changes of inertia properties and aerodynamic properties [32, 33].

Aircraft structural damages are usually accompanied with actuator faults. Loss of control surface areas will reduce the corresponding control effectiveness. Besides, new control derivatives will also be induced if asymmetric damages are imposed on the control surfaces. The way of modelling these effects has been discussed in Sec.III.B.

The aircraft dynamics modeled by Eq. (45) assume the consistency of aircraft center of mass (c.m.) with the body-fixed frame origin. Since sudden structural damages lead to instantaneous c.m. shifts and inertia changes, a more rigorous dynamic modeling method named as non-c.m. approach [33] is adopted in this paper. The dynamic equations for a damaged aircraft using this non-c.m. approach is given by [33]:

$$\begin{bmatrix} \dot{\boldsymbol{V}} \\ \dot{\boldsymbol{\omega}} \end{bmatrix} = \begin{bmatrix} m'\boldsymbol{I} & \tilde{\boldsymbol{S}}^T \\ \tilde{\boldsymbol{S}} & \boldsymbol{J}' \end{bmatrix}^{-1} \begin{bmatrix} -m'\tilde{\boldsymbol{\omega}}\boldsymbol{V} - \tilde{\boldsymbol{\omega}}\tilde{\boldsymbol{S}}^T\boldsymbol{\omega} + \boldsymbol{F}' \\ -\tilde{\boldsymbol{V}}\tilde{\boldsymbol{S}}^T\boldsymbol{\omega} - \tilde{\boldsymbol{\omega}}\tilde{\boldsymbol{S}}\boldsymbol{V} - \tilde{\boldsymbol{\omega}}\boldsymbol{J}'\boldsymbol{\omega} + \boldsymbol{M}' \end{bmatrix} \tag{51}$$

where $\tilde{\boldsymbol{S}}$ is the first moments of inertia matrix.

The aerodynamic properties of partially damaged aircraft have been investigated in [32]. The main influences of wing, horizontal stabilizer and vertical tail damages on aerodynamic coefficients are summarized in Table 1. C_{L_α} in Table 1 is the lift-curve slope, and the new coefficients ΔC_{l_q}, $\Delta C_l(\alpha)$ are caused by geometric asymmetrical damages imposed on the aircraft.

Table 1 The main influences of structural damages on aerodynamic coefficients.

Damaged component	Changed coefficients	New coefficients
Horizontal stabilizer	C_{m_α}, C_{m_q}	ΔC_{l_q}
Vertical tail	C_{n_β}, C_{n_r}	-
Wing	C_{L_α}, C_{l_β}, C_{l_p}	ΔC_{l_q}, $\Delta C_l(\alpha)$

D. Aircraft Attitude Control Design

In this subsection, the aircraft attitude control problem will be considered. The controlled attitude angles are chosen as $\boldsymbol{y} = \boldsymbol{x}_1 = [\phi, \theta, \beta]^T$. Choosing $\boldsymbol{x}_2 = \boldsymbol{\omega} = [p, q, r]^T$, and $\boldsymbol{u} = [\delta_a, \delta_e, \delta_r]$, then Eqs. (48, 50, 51) can be written in a more compact form as:

$$\begin{aligned} \dot{\boldsymbol{x}}_1 &= \boldsymbol{f}_1(\boldsymbol{x}_1) + \boldsymbol{G}_1(\boldsymbol{x}_1)\boldsymbol{x}_2 \\ \dot{\boldsymbol{x}}_2 &= \boldsymbol{f}_2(\boldsymbol{x}_1, \boldsymbol{x}_2) + \boldsymbol{G}_2(\boldsymbol{x}_1, \boldsymbol{x}_2)\boldsymbol{u} \end{aligned} \tag{52}$$

In view of Eqs. (48, 50), the kinematics for $\boldsymbol{x}_1$ is unaffected by faults, model uncertainties and disturbances. On the other hand, the aircraft dynamic equations change from Eq. (45) to Eq. (51) after structural damage occurs, and the aerodynamic coefficients in $\boldsymbol{f}_2$, $\boldsymbol{G}_2$ are perturbed by uncertainties, faults and disturbances. Therefore, the aircraft attitude dynamics modeled by Eq. (52) belong to Eq. (1), so the controllers designed in Sec. II can then be directly applied to this control problem.

IV. Numerical Validation

In this section, the robustness of BS, BSMC and IBSMC will be numerically tested by evaluating their ability of passively tolerating faults and uncertainties. The nominal aerodynamic, thrust and inertia models are set up using the public data of F-16 [34]. It is noteworthy that this aerodynamic data for pitching moment coefficient is non-affine in δ_e, which results in insolvable control problem for BS and BSMC. IBSMC and IBS are able to solve non-affine in the control problems, because Eq. (17) takes partial derivatives with respect to $\boldsymbol{u}$. For fair comparisons, an affine in δ_e model approximated using polynomial functions [9] are consistently used by all the controllers.

The dynamics of rudder, ailerons and stabilators are all modeled as first-order systems. The bandwidth and limits for the actuators are listed in Table 2. A simple proportional-integral thrust control is designed in a separate control loop to maintain airspeed. This aircraft is initially trimmed at a steady level flight condition with airspeed V = 500 ft/s and altitude h = 10,000 ft. The sampling frequency used by the controllers is f_s = 100 Hz.

Table 2 Limits and bandwidths of actuators.

Actuators	Bandwidth [rad/s]	Rate limit [deg/s]	Position limit [deg]
Ailerons δ_a	20.2	80	± 21.5
Elevator δ_e	20.2	90	± 25
Rudder δ_r	20.2	120	± 30

The main focus of this paper is on the comparisons of different control structures, which is independent of specific $\boldsymbol{\nu}_c$ and $\boldsymbol{\nu}_s$ designs. For fair comparisons, gain matrices $\boldsymbol{K}_1 = \text{diag}([2, 2, 2])$ (in Eq. (4)), and $\boldsymbol{K}_2 = \text{diag}([5, 5, 5])$ (in Eqs. (13, 20)) are consistently used by all the controllers. The $\boldsymbol{\nu}_s$ for BSMC and IBSMC are both designed using FRTC SMC method, with $\boldsymbol{\sigma} = \boldsymbol{z}_n$. The SMC parameters used by both BSMC and IBSMC (in Eq. (24)) are $\boldsymbol{K}_s = \text{diag}([0.5, 0.5, 0.1])$ and $\gamma_i = 0.3,\ \ i = 1, 2, 3$. The control performance with varied $\boldsymbol{K}_s$ and γ_i will also be analyzed in the following contexts.

A. Flight Control in the Nominal Case

The references for ϕ and θ are smoothly combined sigmoid functions as continuous and differentiable realizations of 3211 signals. As can be seen from Fig. 1, $|\phi_r| = 20°$, and $|\theta_r - \theta_*| = 15°$, where θ_* is the pitch angle in the trim condition. $\beta_r = 0°$ to minimize the side force during maneuvers.

Fig. 1 shows that all the three controllers, BS, BSMC and IBSMC are able to steer the aircraft to follow the commands. Only small tracking errors present in transition phases, and they are all ultimately bounded. The control surface deflections are smooth. IBSMC has slightly better performance than BS and BSMC as can be seen from the tracking error responses.

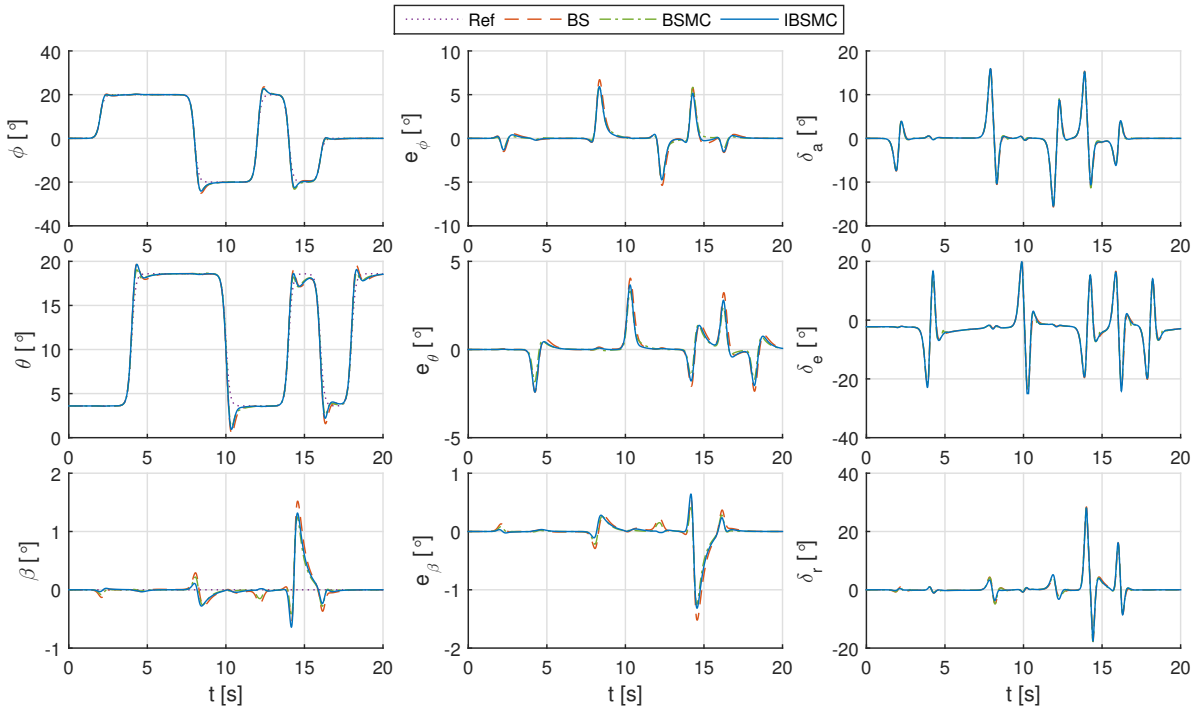

Fig. 1 Aircraft responses and control inputs in the nominal condition.

B. Flight Control in the Presence of Model Uncertainties

In this subsection, the robustness of the controllers to uncertainties will be evaluated. The attitude references are the same as references in the nominal case. Parametric uncertainties are added to the nonlinear system. Specifically, the inertia parameters $J_{xx}, J_{yy}, J_{zz}, J_{xz}$, the damping coefficients $C_{y_r}, C_{y_p}, C_{n_r}, C_{n_p}, C_{l_r}, C_{l_p}, C_{z_q}, C_{m_q}, C_{x_q}$, the control effectiveness $C_{l_{\delta_a}}, C_{l_{\delta_r}}, C_{n_{\delta_a}}, C_{n_{\delta_r}}, C_{y_{\delta_a}}, C_{y_{\delta_r}}$, and the coefficients $C_x(\alpha, \delta_e, M), C_z(\alpha, \delta_e, M), C_m(\alpha, \delta_e, M)$, $C_y(\alpha, \beta, M), C_l(\alpha, \beta, M), C_n(\alpha, \beta, M)$ are multiplied with random combinations of scaling factors, which are in the range of $[0.2, 2]$. The aircraft responses in the presence of uncertainties are shown in Fig. 2, from which it can be seen IBSMC has the best tracking performance. Furthermore, the tracking errors using all these three controllers are ultimately bounded.

In view of Fig. 3, $\|\boldsymbol{I} - \boldsymbol{G}_n \bar{\boldsymbol{G}}_n^{-1}\| < 1$ in this simulation case, and the bounds of $\boldsymbol{\varepsilon}_{ibs}$ are smaller than that of $\boldsymbol{\varepsilon}_{bs}$ in all the three control channels. This result is in accordance with the analyses in subsection II.E, that $\exists \Delta t, s.t. \|\boldsymbol{\varepsilon}_{ibs}\| < \|\boldsymbol{\varepsilon}_{bs}\|$ in the pre-fault condition. By fully exploring the measurements, IBSMC has improved robustness than BSMC.

For the responses shown in Fig. 2, the $\boldsymbol{\nu}_s$ for BSMC and IBSMC are identically designed using FRTC SMC, with the same parameters $\boldsymbol{K}_s$ and γ_i. It can be seen from Fig. 2 that BSMC using these parameters only brings minor performance improvements to standard backstepping. Recall Eq. (24), the DOA of σ_i can be reduced by increasing $K_{s,i}$ and reducing γ_i. The $\boldsymbol{\nu}_s$ in Eq. (23) using difference parameters are illustrated in Fig. 4.

Fig. 5 depicts the influences of SMC gains on the tracking performance of BSMC, where the gain matrix $\boldsymbol{K}_s$ is multiplied with successively increased coefficient $c = 1, 3, 5$, while $\gamma_i = 0.3$ is consistently used. As can be seen from the left subplot of Fig. 4, the increased gains amplify the control effort of $\boldsymbol{\nu}_s$, which can consequently improve the

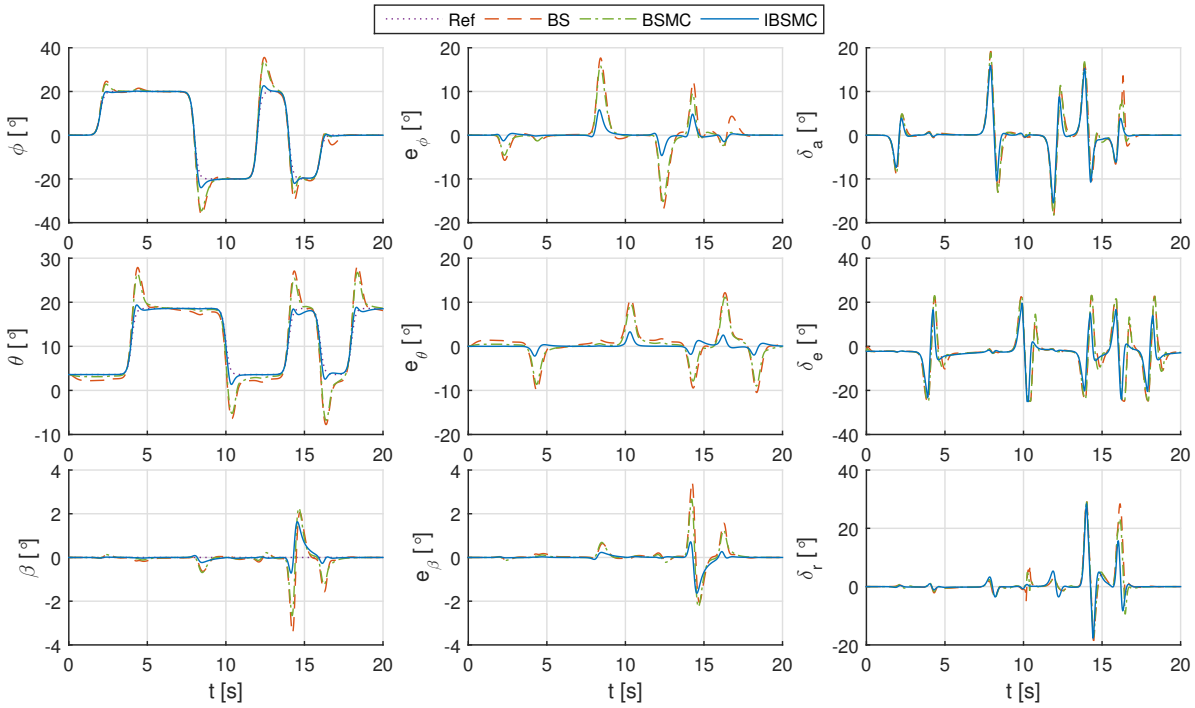

Fig. 2 Aircraft responses and control inputs in the presence of model uncertainties.

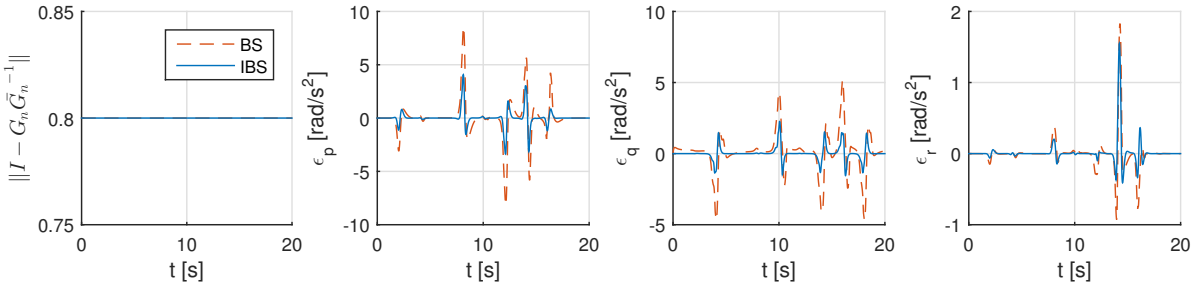

Fig. 3 Responses of $\|I - G_n\bar{G}_n^{-1}\|$ and ε_{bs}, ε_{ibs} in the presence of model uncertainties.

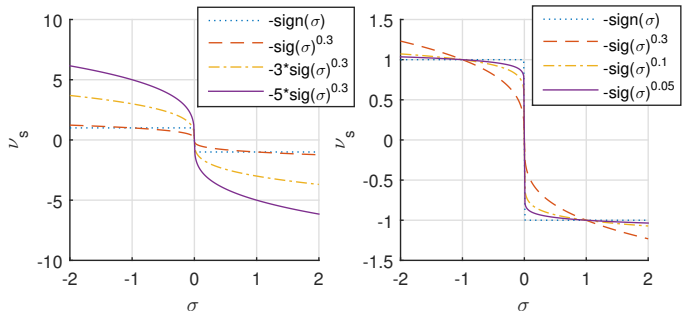

Fig. 4 The FRTC SMC input ν_s (Eq. (23)) with different parameters.

tracking performance of BSMC as verified by Fig. 5. However, high-gain control not only amplifies the measurement noise in practice, but can also impose unachievable commands on actuators. Since actuators have bandwidth and nonlinear limits, high-gain control would induce oscillations and potential instabilities, which is verified in Fig. 5 for the

$c = 5$ case. Moreover, BSMC using five-times higher gains than IBSMC still has inferior robust performance than IBSMC, which can be seen by comparing Fig. 5 with Fig. 2.

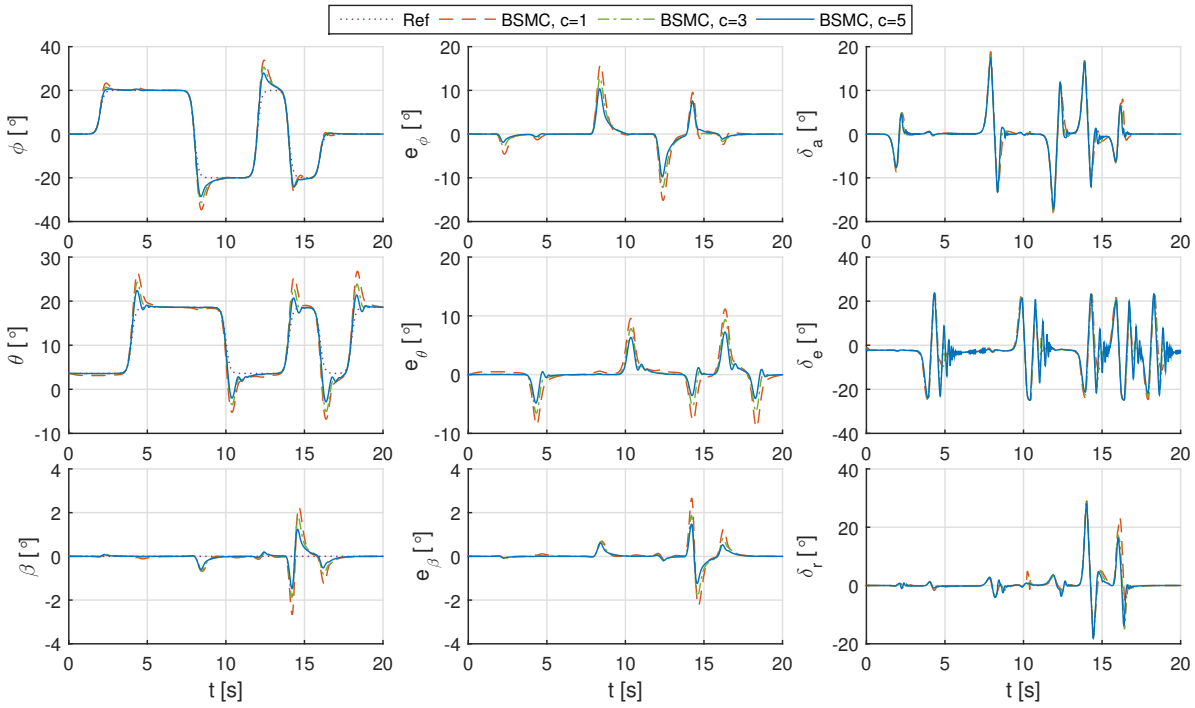

Fig. 5 The influences of SMC gains on the tracking performance of BSMC.

The DOA of σ_i can also be reduced by diminishing γ_i (Eq. (24)). As shown by Eq. (23) and the right subplot of Fig. 4, $\text{sig}(\sigma)^\gamma = |\sigma|^\gamma \text{sign}(\sigma)$ becomes steeper near $\sigma = 0$ as γ approaches zero, which can speed up the convergence near the sliding surface. This is verified by the tracking performance of BSMC using varies γ shown in Fig. 6. However, if $\gamma = 0$, then $\text{sig}(\sigma)^\gamma = \text{sign}(\sigma)$, which means although the $\boldsymbol{\nu}_s$ designed by Eq. (23) is continuous, chattering would present if sufficiently small γ is used. This phenomenon is verified in Fig. 6 by the $\gamma = 0.05$ case. Therefore, trade-offs should be made between performance and chattering reduction. Furthermore, the robust performance of IBSMC is better than BSMC using all the tested γ values, which can be seen by comparing Fig. 6 with Fig. 2.

C. Flight Control in the Presence of Actuator Faults

In this subsection, the robustness of BS, BSMC, and IBSMC will be tested by their abilities of passively resisting actuator faults. The actuator fault scenarios considered in this subsection satisfy $|\boldsymbol{G}_2(\boldsymbol{x}, \kappa)| \neq 0$, which means the pitch, roll, and yaw channels are still controllable after faults. Nevertheless, the control authorities reduce after actuator fault occurs. In view of the control authority losses, the attitude references are halved here as compared to the nominal condition. specifically, $|\phi_r| = 10°$, $|\theta_r - \theta_*| = 7.5°$, $\beta_r = 0°$. The influences of actuator faults are modeled using methods introduced in Sec. III.B.

The first actuator fault scenario considered is a combination of aileron and rudder faults. Specifically, at $t = 3$ s, the right aileron runs away and get jammed at $\delta_{a,r\Delta} = 10°$, while the rudder suddenly lost 50% of its effectiveness at $t = 7$ s. The sign for aileron deflection angles are defined in the conventional way, namely a positive δ_a means the right aileron deflects downwards while the left deflects upwards.

According to the discussions in subsection III.B, in this scenario, the control effectiveness of ailerons and rudder are halved, and new control derivative $C_{m_{\delta_a}}$ is induced. Because the right aileron is jammed at a non-neutral position $\delta_{a,r\Delta} = 10°$, extra negative rolling and pitching moment coefficients are induced. This can be seen from the aircraft responses using BS and BSMC shown in Fig. 7, that the aircraft rolls to the left and pitches down after $t = 3$ s. If $\boldsymbol{\varepsilon}_{bs}$ in Eq. (14) is bounded, backstepping control itself can guarantee the ultimately boundedness of the tracking errors. However, over 20° of roll angle tracking error presents after $t = 3$ s, noticeable tracking errors for θ and β also appear in Fig. 7.

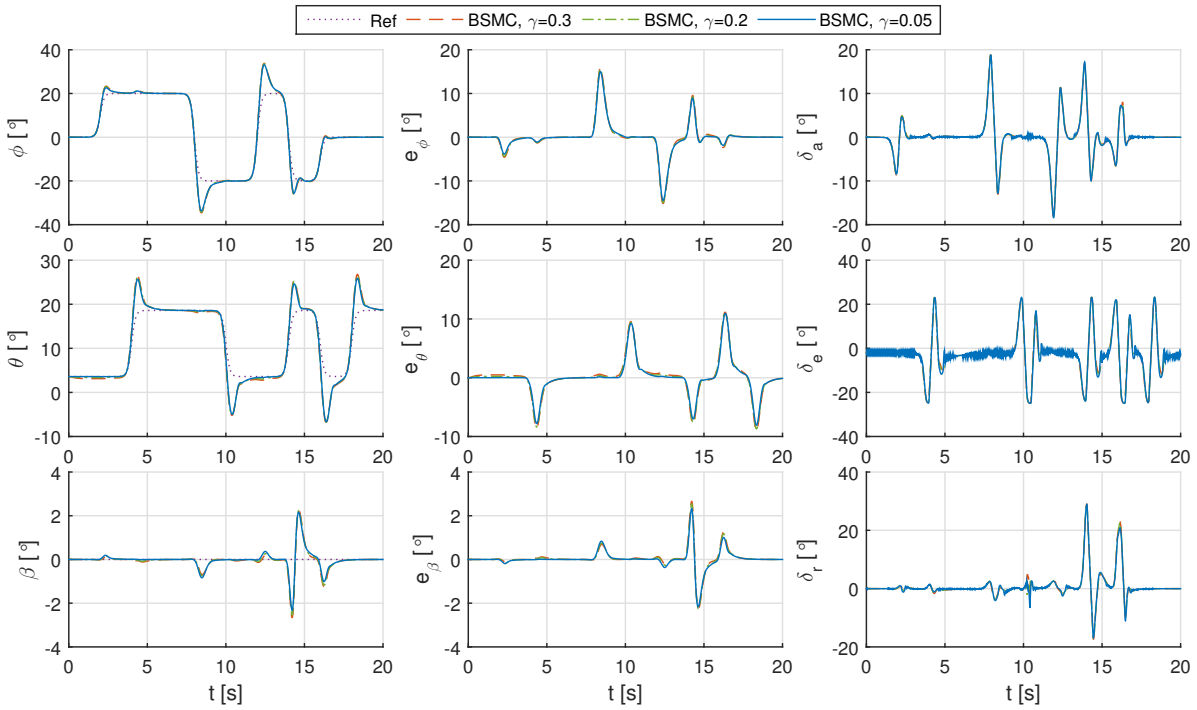

Fig. 6 The influences of SMC parameter γ on the tracking performance of BSMC.

The BSMC and IBSMC in Fig. 7 use the same set of parameter: $\boldsymbol{K}_s = \text{diag}([0.5, 0.5, 0.1])$ and $\gamma_i = 0.3,\ \ i = 1, 2, 3$. Although BSMC brings performance improvements to backstepping, its robustness is still inferior than IBSMC. It can be seen from Fig. 7 that aircraft using IBSMC is able to passively recover from the fault within seconds, with marginal tracking errors. The left aileron rapidly deflects downwards at $\delta_{a,l\Delta} = -10^\circ$ to compensate for the right aileron jamming induced moments after $t = 3$ s.

Inheriting the robustness of both IBS and SMC, IBSMC shows the best robust performance in Fig. 7. It has been revealed in Sec. II.E, that the closed-loop uncertainty under IBS control naturally has smaller bound than the uncertainty bound using backstepping control, both before and after fault occurs. This conclusion is further verified in Fig. 8, in which $\|\boldsymbol{\varepsilon}_{ibs}\| < \|\boldsymbol{\varepsilon}_{bs}\|$ during the entire time history. Moreover, $|\boldsymbol{\varepsilon}_{bs,p}|$ and $|\boldsymbol{\varepsilon}_{bs,r}|$ have biases after $t = 3$ s, while $|\boldsymbol{\varepsilon}_{ibs,p}|$ and $|\boldsymbol{\varepsilon}_{ibs,r}|$ consistently fluctuating around zero. $\|\boldsymbol{I} - \boldsymbol{G}_n\bar{\boldsymbol{G}}_n^{-1}\| < 1$ is satisfied under both BS and IBS control, which ensures the boundedness of $\boldsymbol{\varepsilon}_{ibs}$ if other conditions in Theorem 1 are also satisfied. The sudden changes of $\|\boldsymbol{I} - \boldsymbol{G}_n\bar{\boldsymbol{G}}_n^{-1}\|$ in Fig. 8 are caused by the sudden effectiveness losses, and the variations of $\|\boldsymbol{I} - \boldsymbol{G}_n\bar{\boldsymbol{G}}_n^{-1}\|$ are because $\boldsymbol{G}_n$ is a function of states.

The second actuator fault scenario is that the left stabilator suffers from solid Oscillatory Failure Case (OFC) from $t = 5$ s. Based on the modeling method introduced in Sec. III.B, the deflection of the left stabilator after fault is modeled as $\delta_{e,l} = 10\sin(2(t-5))\ (^\circ),\ t \geq 5$ s. The right stabilator is still under control. As a result, $C_{m_{\delta_e}}$ is halved, new control derivatives $C_{l_{\delta_e}}$ and $C_{n_{\delta_e}}$ are also induced. The disturbing force and moment coefficients caused by the solid OFC significantly deteriorate the tracking performance of backstepping as shown in Fig. 9. IBSMC shows the best performance over backstepping and BSMC in all the three control channels.

$\|\boldsymbol{I} - \boldsymbol{G}_n\bar{\boldsymbol{G}}_n^{-1}\| < 1$ is satisfied in this scenario as shown in Fig. 10. Moreover, it is illustrated in Fig. 10 that $\|\boldsymbol{\varepsilon}_{ibs}\| < \|\boldsymbol{\varepsilon}_{bs}\|$ during the entire time history. It is worth noting that $\|\boldsymbol{\varepsilon}_{ibs}\|$ can be further reduced by increasing the sampling frequency, while $\|\boldsymbol{\varepsilon}_{bs}\|$ is independent of Δt. Since $\|\boldsymbol{\varepsilon}_{ibs}\|$ is smaller, IBSMC using the same SMC parameters as BSMC also has smaller DOA (Eq. (24)), which consequently leads to the better robust performance of IBSMC, which is verified in Fig. 9.

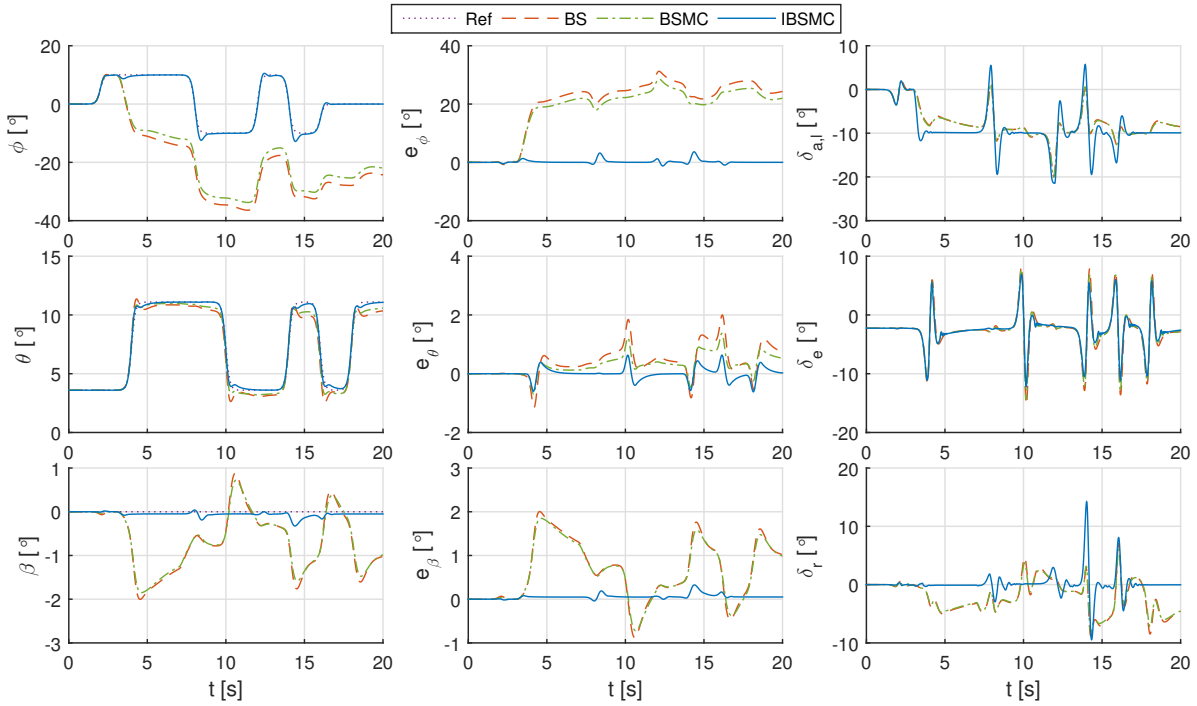

Fig. 7 Aircraft responses and control inputs with aileron, rudder faults occur at $t = 3,\ 7$ s.

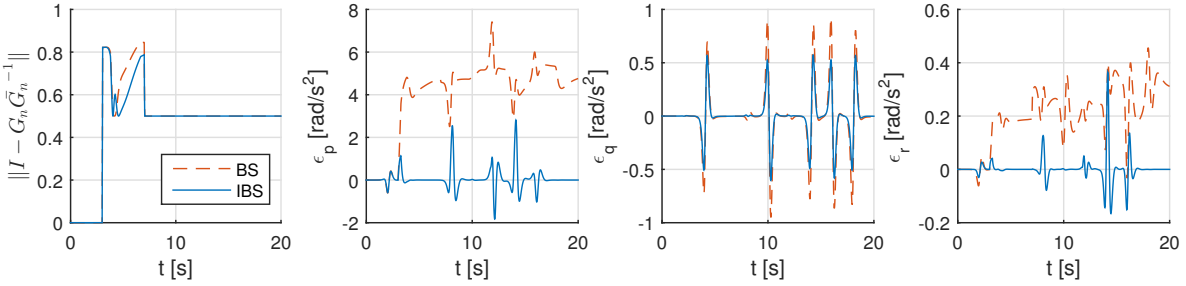

Fig. 8 Responses of $\|\boldsymbol{I} - \boldsymbol{G}_n\bar{\boldsymbol{G}}_n^{-1}\|$ and $\boldsymbol{\varepsilon}_{bs},\ \boldsymbol{\varepsilon}_{ibs}$ in the presence of aileron and rudder faults occur at $t = 3,\ 7$ s.

D. Flight Control in the Presence of Structural Damages

In this subsection, the robustness of BS, BSMC, and IBSMC will be tested by their abilities of passively resisting structural damages. The damaged aircraft is unable to execute severe maneuvers, because of its shrunken flight envelop. Therefore, the attitude references are halved in this subsection as compared to the nominal case, namely, $|\phi_r| = 10°$, $|\theta_r - \theta_*| = 7.5°$, $\beta_r = 0°$. The influences of structural damages are modeled using methods introduced in Sec. III.C. The inertia properties of the damaged aircraft is calculated using a CATIA model of F-16.

The first structural damage scenario considered is that the right wing lost 25% of its area at $t = 3$ s. Accompanying with the wing area loss, the entire right aileron is also lost. A positive rolling moment caused by the unequal lifts on the left and right wings significantly degrades the roll angle tracking performance of BS and BSMC, as shown by Fig. 11. e_θ and e_β also increase under BS and BSMC control owing to the coupling effects. By contrast, aircraft using IBSMC is able to tolerant these faults passively, and has the smallest tracking error variations. In view of Fig. 11, the positive rolling moment is timely compensated by the upwards deflections of the left aileron using IBSMC.

As consistent with the theoretical analyses in Sec. II.E, and the responses in the presence of actuator faults in Sec. IV.C, $\|\boldsymbol{\varepsilon}_{ibs}\| < \|\boldsymbol{\varepsilon}_{bs}\|$ also holds in this wing damage case as illustrated by Fig. 12. $\|\boldsymbol{I} - \boldsymbol{G}_n\bar{\boldsymbol{G}}_n^{-1}\| < 1$ is satisfied under both BS and IBS control in this scenario.

The second structural damage scenario is a combination of wing, stabilator and vertical tail damages. To be specific,

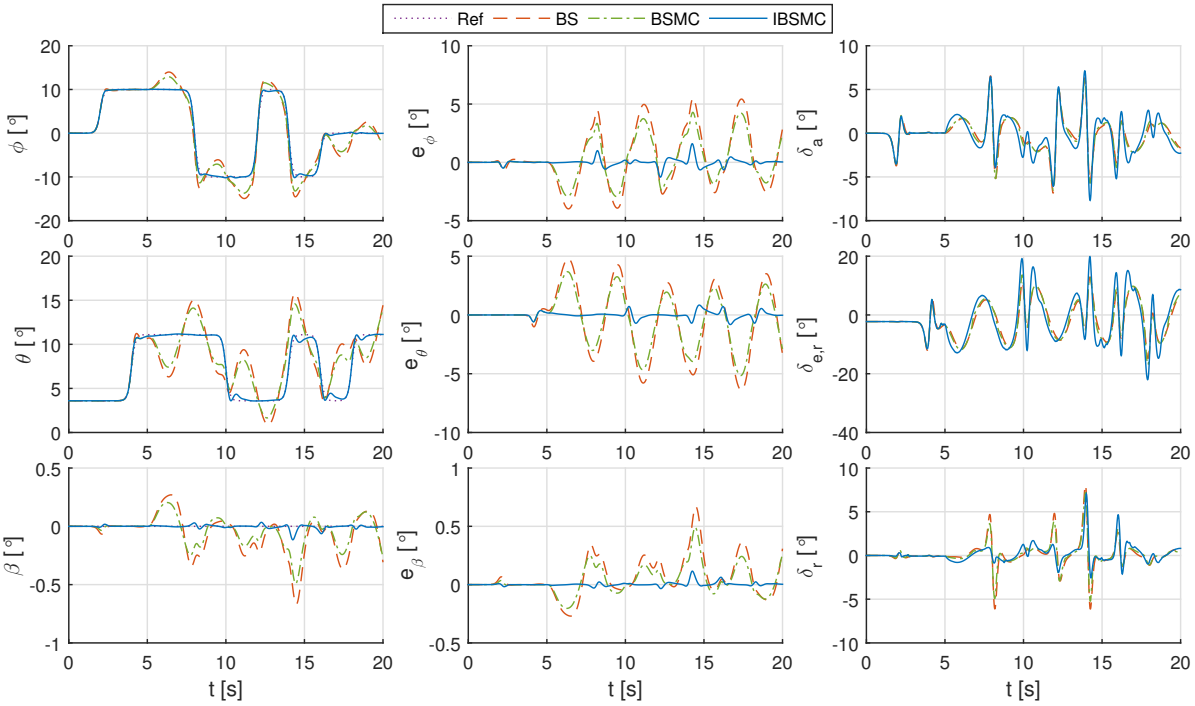

Fig. 9 Aircraft responses and control inputs with a stabilator solid OFC fault occurs at $t = 5$ s.

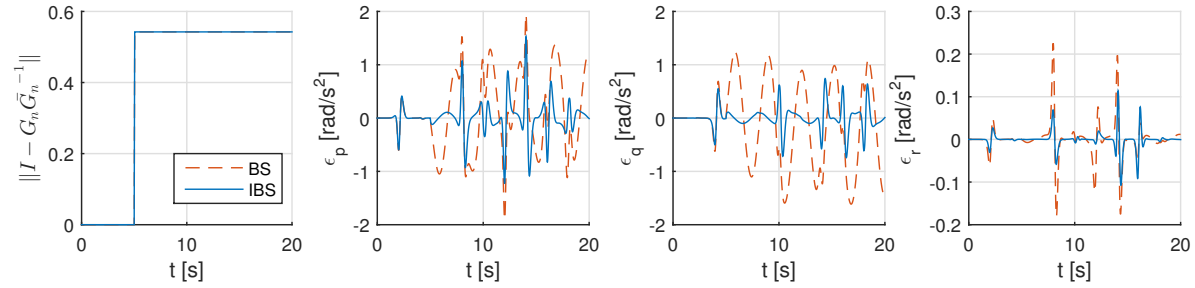

Fig. 10 Responses of $\|I - G_n\bar{G}_n^{-1}\|$ and ε_{bs}, ε_{ibs} with a stabilator solid OFC fault occurs at $t = 5$ s.

the right wing lost 25% of its area at $t = 3$ s. Afterwards, the entire left stabilator is lost at $t = 5$ s. Subsequently, one half area of the vertical tail is lost at $t = 7$ s. Accompanying with the structural damages, the corresponding control surfaces are also lost. The aircraft responses and control inputs using BS, BSMC, and IBSMC are shown in Fig. 13, from which it can be seen IBSMC has the best tracking accuracy. Although the tracking errors using BSMC and BS are ultimately bounded, remarkable performance deteriorations present in Fig. 13.

The conclusion that $\boldsymbol{\varepsilon}_{ibs}$ has smaller bound than $\boldsymbol{\varepsilon}_{bs}$ is further verified in Fig. 14 for the comprehensive structural damage scenario. As a result, IBSMC using the same $\boldsymbol{\nu}_s$ design as BSMC has remarkable performance enhancements.

Analogous to the discussions in Sec. IV.B, the performance of BSMC can be improved by reducing γ and increasing $\boldsymbol{K}_s$. It has been shown in Fig. 6 that chattering effects would present as γ approaching zero. Fig. 15 shows the tracking responses of an aircraft using BSMC in the second structural damage scenario with gradually increased gains $\boldsymbol{K}_s = c \cdot \mathrm{diag}([0.5, 0.5, 0.1])$. It can be seen from Fig. 15 that high-gain BSMC can indeed enhance the tracking performance, but will cause oscillations owing to the actuator limits, and will also amplify measurement noise in practice. By contrast, IBSMC with much lower SMC gains is able to provide satisfactory tracking performance in spite of structural damages as illustrated in Fig. 13.

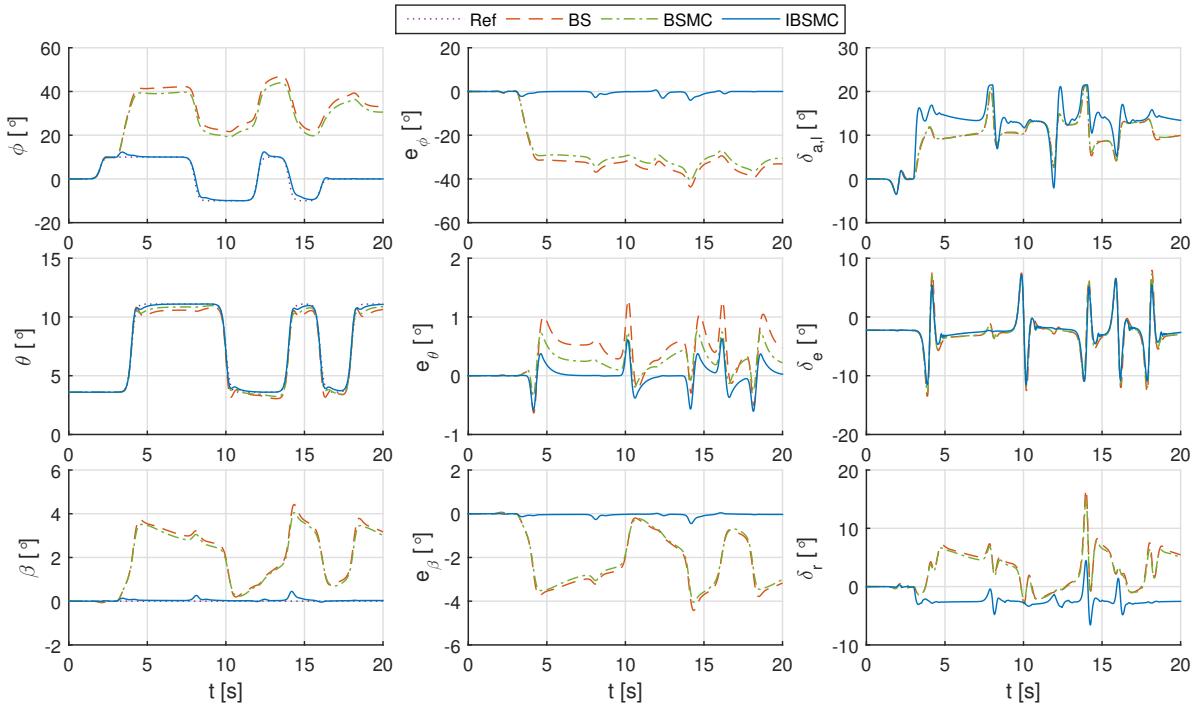

Fig. 11 Aircraft responses and control inputs when 25% of the wing area lost at $t = 3$ s.

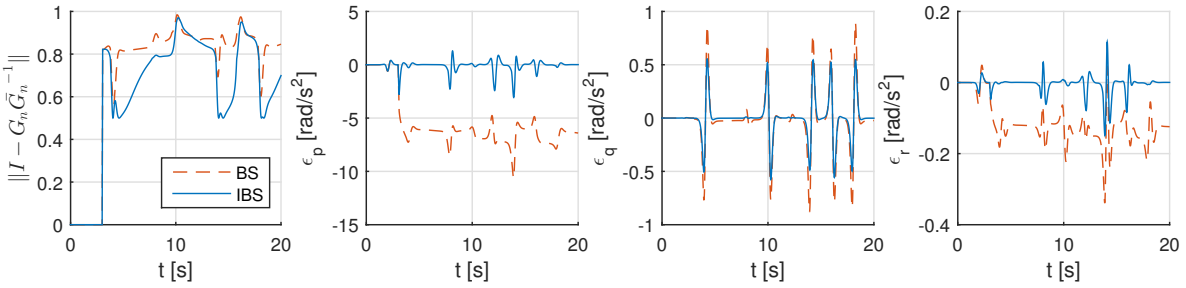

Fig. 12 Responses of $\|\boldsymbol{I} - \boldsymbol{G}_n\bar{\boldsymbol{G}}_n^{-1}\|$ and $\boldsymbol{\varepsilon}_{bs}$, $\boldsymbol{\varepsilon}_{ibs}$ in a wing damage (from $t = 3$ s) circumstance.

V. Conclusions

The Incremental Backstepping Sliding Mode Control (IBSMC) framework for multi-input/output nonlinear strict-feedback systems under the perturbations of model uncertainties, sudden faults, and external disturbances is proposed in this paper. Inheriting the merits of both Incremental Backstepping (IBS) and Sliding Model Control (SMC), this framework has shown enhanced robust performance as compared to backstepping and SMC hybridized with backstepping (BSMC). Tuning of IBSMC is straightforward, and is easier than Adaptive Backstepping (ABS). IBSMC also has less model dependency than BSMC, which simplifies the implementation process and reduces the computational load.

It is proved by Theorem 1 that a diagonal dominate structure of $\boldsymbol{G}_n\bar{\boldsymbol{G}}_n^{-1}$, bounded $\boldsymbol{\delta}_\kappa(\boldsymbol{x})$ at the fault instant, and a sufficiently high sampling frequency f_s guarantee the uncertainty vector remains in the closed-loop system under IBS control ($\boldsymbol{\varepsilon}_{ibs}$) is bounded, while the remaining closed-loop uncertainty term using backstepping control ($\boldsymbol{\varepsilon}_{bs}$) is undetermined under the same conditions. Moreover, for fault and disturbance circumstances where both $\boldsymbol{\varepsilon}_{ibs}$ and $\boldsymbol{\varepsilon}_{bs}$ are bounded, there exists an f_s that ensures $\boldsymbol{\varepsilon}_{ibs}$ has smaller bound, both before and after a fault occurs. This smaller bound of $\boldsymbol{\varepsilon}_{ibs}$ allows IBSMC to passively resist a wider range of perturbations using not only less model information, but also reduced SMC gains.

For solving the aircraft fault-tolerant control problem, the SMC virtual controls in BSMC and IBSMC are consistently designed using the Finite Reaching Time Continuous (FRTC) SMC method. Numerical simulations verify that IBSMC

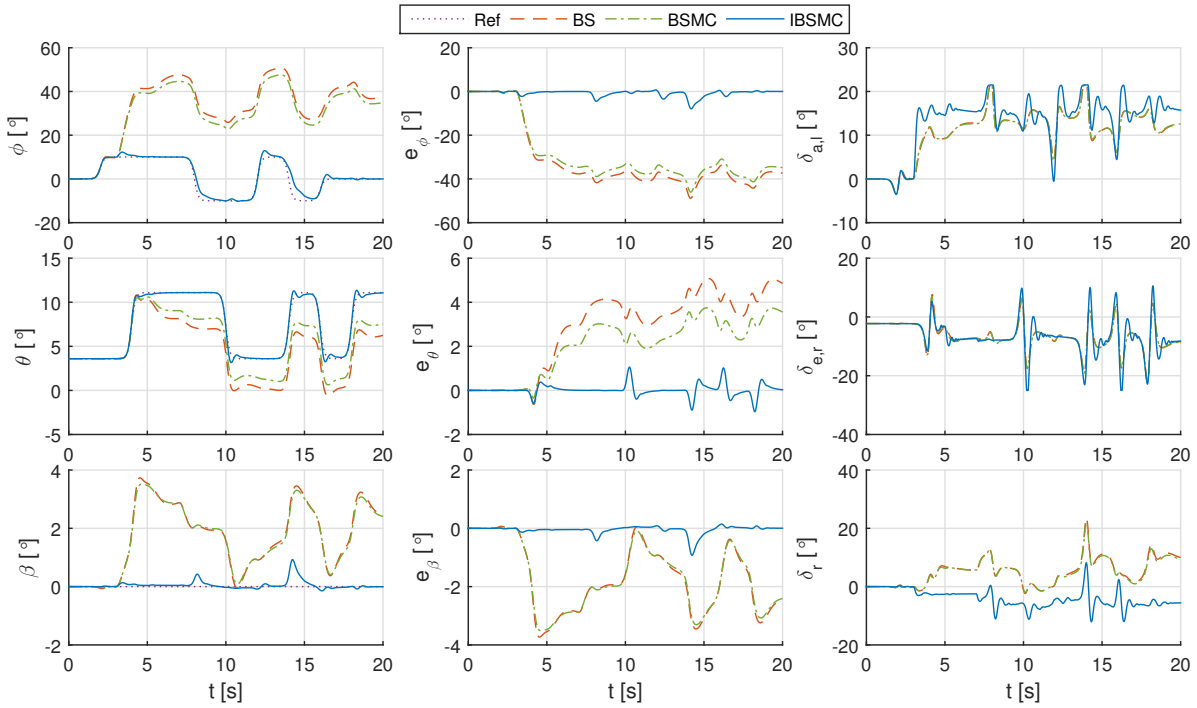

Fig. 13 Aircraft responses and control inputs with wing, stabilator and vertical tail damaged at $t = 3,\ 5,\ 7$ s.

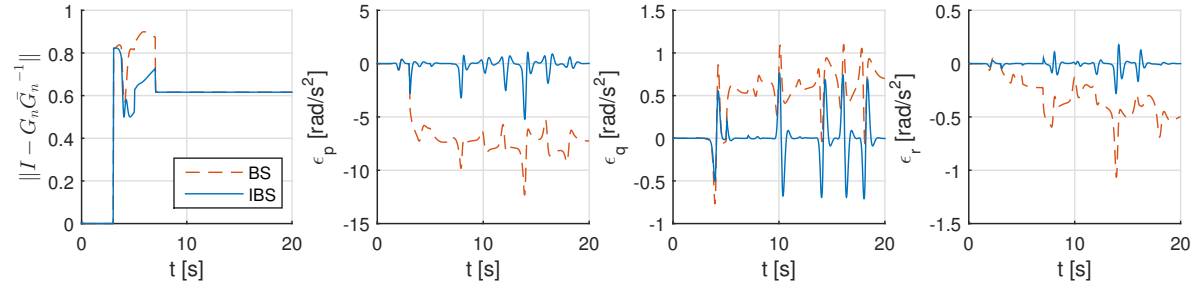

Fig. 14 Responses of $\|I - G_n\bar{G}_n^{-1}\|$ and $\varepsilon_{bs},\ \varepsilon_{ibs}$ with wing, stabilator and vertical tail damaged at $t = 3,\ 5,\ 7$ s.

has improved robust performance over backstepping and BSMC, in the presence of model uncertainties, sudden actuator faults and structural damages. In conclusion, easier implementation, less model dependency, and better robustness make the proposed IBSMC framework promising for enhancing aircraft survivability in real life.

References

[1] "Statistical Summary of Commercial Jet Airplane Accidents," Tech. rep., Boeing Commercial Airplanes, 2015. URL `http://www.boeing.com/commercial/safety/investigate.html`.

[2] "Annual Safety Review 2017," Tech. rep., European Aviation Safety Agency, 2017. doi:10.2822/541561.

[3] Russell, P., and Pardee, J., "Joint Safety Analysis Team-CAST Approved Final Report Loss of Control JSAT Results and Analysis," Tech. rep., Federal Aviation Administration: Commercial Airline Safety Team, 2000.

[4] Khalil, H. K., *Nonlinear Systems*, Prentice-Hall, New Jersey, 2002.

[5] Slotine, J.-J. E., and Li, W., *Applied Nonlinear Control*, NJ: Prentice hall, Englewood Cliffs, 1991.

[6] Astolfi, A., and Ortega, R., "Immersion and invariance: A new tool for stabilization and adaptive control of nonlinear systems," *IEEE Transactions on Automatic Control*, Vol. 48, No. 4, 2003, pp. 590–606. doi:10.1109/TAC.2003.809820.

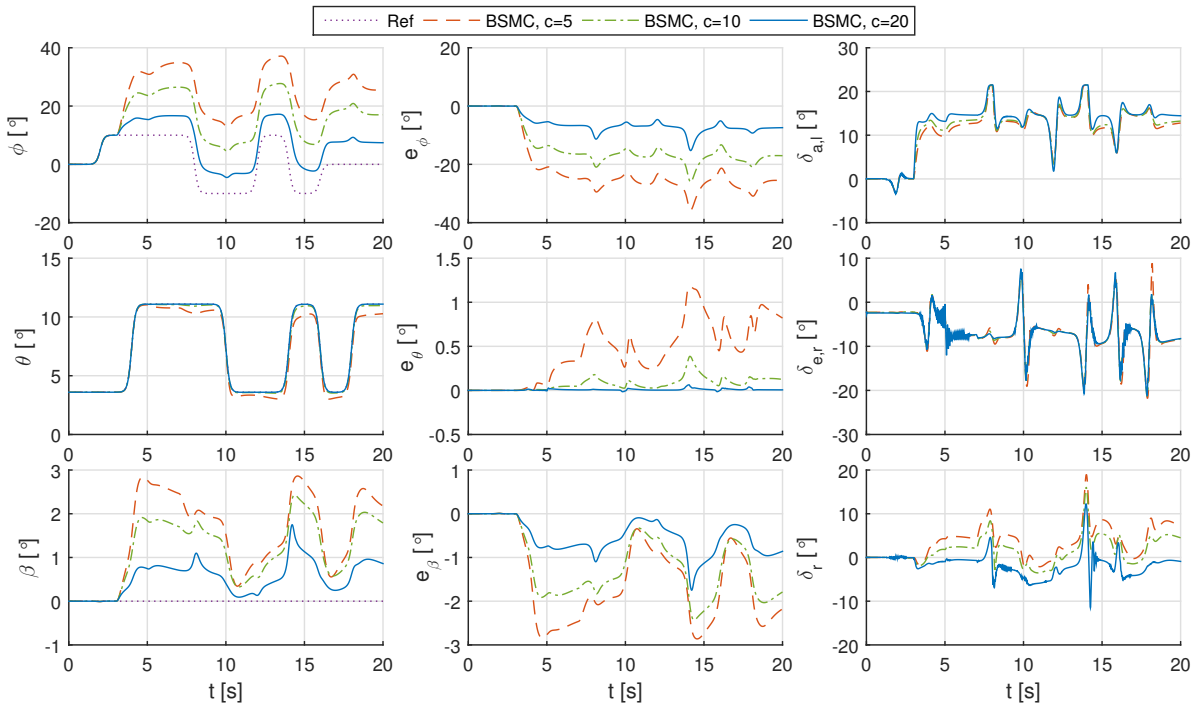

Fig. 15 The influences of the SMC gains on the tracking performance of BSMC in a structural damage scenario.

[7] Ikhouane, F., and Krstić, M., "Robustness of the tuning functions adaptive backstepping design for linear systems," *IEEE Transactions on Automatic Control*, Vol. 43, No. 3, 1998, pp. 431–437. doi:10.1109/9.661616.

[8] Bartolini, G., Ferrara, A., Giacomini, L., and Usai, E., "Properties of a combined adaptive/second-order sliding mode control algorithm for some classes of uncertain nonlinear systems," *IEEE Transactions on Automatic Control*, Vol. 45, No. 7, 2000, pp. 1334–1341. doi:10.1109/9.867041.

[9] van Gils, P., Van Kampen, E., de Visser, C. C., and Chu, Q. P., "Adaptive Incremental Backstepping Flight Control for a High-Performance Aircraft with Uncertainties," *AIAA Guidance, Navigation, and Control Conference*, American Institute of Aeronautics and Astronautics, San Diego, California, 2016. doi:10.2514/6.2016-1380, URL `http://arc.aiaa.org/doi/10.2514/6.2016-1380`.

[10] Cong, B., Liu, X., and Chen, Z., "Backstepping based adaptive sliding mode control for spacecraft attitude maneuvers," *Aerospace Science and Technology*, Vol. 30, No. 1, 2013, pp. 1–7. doi:10.1016/j.ast.2013.05.005, URL `http://dx.doi.org/10.1016/j.ast.2013.05.005`.

[11] Shtessel, Y. B., Buffington, J. M., and Banda, S. S., "Multiple Timescale Flight Control Using Reconfigurable Sliding Modes," *Journal of Guidance, Control, and Dynamics*, Vol. 22, No. 6, 1999, pp. 873–883. doi:10.2514/2.4465.

[12] Hall, C. E., and Shtessel, Y. B., "Sliding Mode Disturbance Observer-Based Control for a Reusable Launch Vehicle," *Journal of Guidance, Control, and Dynamics*, Vol. 29, No. 6, 2006, pp. 1315–1328. doi:10.2514/1.20151.

[13] Sagliano, M., Mooij, E., and Theil, S., "Adaptive Disturbance-Based High-Order Sliding-Mode Control for Hypersonic-Entry Vehicles," *Journal of Guidance, Control, and Dynamics*, Vol. 40, No. 3, 2017, pp. 521–536. doi:10.2514/1.G000675.

[14] Fazeli Asl, S. B., and Moosapour, S. S., "Adaptive backstepping fast terminal sliding mode controller design for ducted fan engine of thrust-vectored aircraft," *Aerospace Science and Technology*, Vol. 71, 2017, pp. 521–529. doi:10.1016/j.ast.2017.10.001, URL `https://doi.org/10.1016/j.ast.2017.10.001`.

[15] Koshkouei, A. J., Zinober, A., and Sheffield, S., "Adaptive Sliding Backstepping Control of Nonlinear Semi-Strict Feedback Form Systems," *Mediterranean Conference on Control and Automation*, , No. February, 1999, pp. 2376–2383.

[16] Scarratt, J. C., Zinober, A., Mills, R. E., Rios-Bolıivar, M., Ferrara, A., and Giacomini, L., "Dynamical Adaptive First and Second-Order Sliding Backstepping Control of Nonlinear Nontriangular Uncertain Systems," *Journal of Dynamic Systems, Measurement, and Control*, Vol. 122, No. 4, 2000, p. 746. doi:10.1115/1.1321051, URL http://dynamicsystems.asmedigitalcollection.asme.org/article.aspx?articleid=1408750.

[17] Jia, Z., Yu, J., Mei, Y., Chen, Y., Shen, Y., and Ai, X., "Integral backstepping sliding mode control for quadrotor helicopter under external uncertain disturbances," *Aerospace Science and Technology*, Vol. 68, 2017, pp. 299–307. doi:10.1016/j.ast.2017.05.022, URL http://dx.doi.org/10.1016/j.ast.2017.05.022.

[18] Sieberling, S., Chu, Q. P., and Mulder, J. A., "Robust Flight Control Using Incremental Nonlinear Dynamic Inversion and Angular Acceleration Prediction," *Journal of Guidance, Control, and Dynamics*, Vol. 33, No. 6, 2010, pp. 1732–1742. doi:10.2514/1.49978.

[19] Lu, P., Van Kampen, E., and Chu, Q., "Robustness and Tuning of Incremental Backstepping Approach," *AIAA Guidance, Navigation, and Control Conference*, American Institute of Aeronautics and Astronautics, Kissimmee, Florida, 2015, pp. 1–15. doi:10.2514/6.2015-1762.

[20] Lu, P., and Van Kampen, E., "Active Fault-Tolerant Control System using Incremental Backstepping Approach," *AIAA Guidance, Navigation, and Control Conference*, American Institute of Aeronautics and Astronautics, Kissimmee, Florida, 2015, pp. 1–17. doi:10.2514/6.2015-1312, URL http://arc.aiaa.org/doi/10.2514/6.2015-1312.

[21] Lu, P., van Kampen, E., de Visser, C. C., and Chu, Q. P., "Framework for Simultaneous Sensor and Actuator Fault-Tolerant Flight Control," *Journal of Guidance, Control, and Dynamics*, Vol. 40, No. 8, 2017, pp. 1–9. doi:10.2514/1.G002079, URL https://arc.aiaa.org/doi/10.2514/1.G002079.

[22] van Ekeren, W., Looye, G., Kuchar, R. O., Chu, Q. P., and Van Kampen, E., "Design, Implementation and Flight-Tests of Incremental Nonlinear Flight Control Methods," *2018 AIAA Guidance, Navigation, and Control Conference*, American Institute of Aeronautics and Astronautics, Kissimmee, Florida, 2018, pp. 1–21. doi:10.2514/6.2018-0384.

[23] Wang, X., Van Kampen, E., Chu, Q. P., and Lu, P., "Stability Analysis for Incremental Nonlinear Dynamic Inversion Control," *2018 AIAA Guidance, Navigation, and Control Conference*, AIAA, Kissimmee, Florida, 2018. doi:10.2514/6.2018-1115.

[24] Brown, M., Shtessel, Y., and Buffington, J., "Finite reaching time continuous sliding mode control with enhanced robustness," *AIAA Guidance, Navigation, and Control Conference and Exhibit*, American Institute of Aeronautics and Astronautics, Denver, CO, 2000. doi:10.2514/6.2000-3964, URL http://arc.aiaa.org/doi/10.2514/6.2000-3964.

[25] Shtessel, Y., Buffington, J., and Banda, S., "Tailless aircraft flight control using multiple time scale reconfigurable sliding modes," *IEEE Transactions on Control Systems Technology*, Vol. 10, No. 2, 2002, pp. 288–296. doi:10.1109/87.987075.

[26] Acquatella, P., van Kampen, E., and Chu, Q. P., "Incremental Backstepping for Robust Nonlinear Flight Control," *CEAS Conference on Guidance, Navigation, and Control*, , No. April 2013, 2013, pp. 1444–1463. doi:10.2541/1.49978.

[27] Hodel, A., Whorton, M., and Zhu, J., "Stability Metrics for Simulation and Flight-Software Assessment and Monitoring of Adaptive Control Assist Compensators," *AIAA Guidance, Navigation and Control Conference and Exhibit*, American Institute of Aeronautics and Astronautics, Honolulu, Hawaii, 2008, pp. 1–25. doi:10.2514/6.2008-7005.

[28] Yu, S., Yu, X., Shirinzadeh, B., and Man, Z., "Continuous finite-time control for robotic manipulators with terminal sliding mode," *Automatica*, Vol. 41, No. 11, 2005, pp. 1957–1964. doi:10.1016/j.automatica.2005.07.001.

[29] Wang, X., van Kampen, E.-J., Chu, Q., and Lu, P., "Incremental Sliding-Mode Fault-Tolerant Flight Control," *Journal of Guidance, Control, and Dynamics*, 2018, pp. 1–16. doi:10.2514/1.G003497, URL https://arc.aiaa.org/doi/10.2514/1.G003497.

[30] Grondman, F., Looye, G., Kuchar, R. O., Chu, Q. P., and Van Kampen, E., "Design and Flight Testing of Incremental Nonlinear Dynamic Inversion-based Control Laws for a Passenger Aircraft," *2018 AIAA Guidance, Navigation, and Control Conference*, AIAA, Kissimmee, Florida, 2018. doi:10.2514/6.2018-0385.

[31] Goupil, P., "Oscillatory failure case detection in the A380 electrical flight control system by analytical redundancy," *IFAC Proceedings Volumes (IFAC-PapersOnline)*, Vol. 17, No. PART 1, 2007, pp. 681–686. doi:10.1016/j.conengprac.2009.04.003.

[32] Shah, G., "Aerodynamic Effects and Modeling of Damage to Transport Aircraft," *AIAA Atmospheric Flight Mechanics Conference and Exhibit*, American Institute of Aeronautics and Astronautics, Honolulu, Hawaii, 2008, pp. 1–13. doi:10.2514/6.2008-6203, URL http://arc.aiaa.org/doi/pdf/10.2514/6.2008-6203http://arc.aiaa.org/doi/10.2514/6.2008-6203.

[33] Bacon, B., and Gregory, I., "General Equations of Motion for a Damaged Asymmetric Aircraft," *AIAA Atmospheric Flight Mechanics Conference and Exhibit*, American Institute of Aeronautics and Astronautics, Hilton Head, South Carolina, 2007, pp. 1–13. doi:10.2514/6.2007-6306, URL http://arc.aiaa.org/doi/pdf/10.2514/6.2007-6306http://arc.aiaa.org/doi/10.2514/6.2007-6306.

[34] Nguyen, L. T., Ogburn, M. E., Gilbert, W. P., Kibler, K. S., Brown, P. W., and Deal, P. L., "Simulator Study of Stall/Post-Stall Characteristics of a Fighter Airplane with Relaxed Longitudinal Static Stability," Tech. Rep. NASA Technical Paper 1538, 1979.